Student thesis series INES nr 361

Locating potential flood areas in an urban environment using remote sensing and GIS, case study Lund, Sweden

Joakim Lindberg

2015
Department of
Physical Geography and Ecosystems Science
Lund University
Sölvegatan 12
S-223 62 Lund
Sweden

Joakim Lindberg (2015). *Locating potential flood areas in an urban environment using remote sensing and GIS, case study Lund, Sweden*
Master degree thesis, 30 credits in *Geomatics*
Department of Physical Geography and Ecosystems Science, Lund University

Level: Master of Science (MSc)

Course duration: *January* 2014 until *June* 2014

Disclaimer

Locating potential flood areas in an urban environment using remote sensing and GIS, case study Lund, Sweden

---

Joakim Lindberg

Master thesis, 30 credits, in *Geomatics*

Supervisor
Thomas Holst

Exam committee:

Harry Lankrejier,
Department of Physical Geography and Ecosystem Science
Lund University

David Tenenbaum,
Department of Physical Geography and Ecosystem Science
Lund University

Abstract

Impervious surfaces within urban areas contribute to reduced infiltration, increased runoff volumes and potential pollution. Modelling flooding in an urban setting is increasingly relevant given the potential risk associated with impervious surfaces. With expanding urban areas and ongoing climate change, having functioning storm water management is an important factor in today's city management. Consideration has to be given to the surface complexities and topography that are presented in an urban environment.

The aim of this study was to develop a method of locating areas in an urban setting with a high potential for flood during, or after, extreme (>40 mm/day) precipitation events. This was done using GIS-based analysis together with remote sensing to create an impervious surface analysis and a runoff model. The result highlights areas believed to have a high risk of flooding in the event of heavy rainfall. The study area is the town of Lund in southern Sweden. The study used an Ortho-image from 2010, provided by the municipality of Lund, as input for an impervious surface analysis. This is used as input to a model which predicts runoff volumes and locates potential flooding areas.

The results indicate that impervious surfaces are a major factor when analysing runoff in an urban environment. Large connected impervious surfaces have the potential to produce large volumes of runoff if not properly drained. The results also indicate that vegetated areas have a great potential to disrupt flow and prevent flooding.

Keywords: Geography, Physical Geography, GIS, Remote Sensing, Impervious surfaces, Extreme events, Urban, Runoff, Storm water, Lund

Sammanfattning

Hårdgjorda ytor i stadsmiljö är en bidragande orsak till reducerad infiltration, ökad avrinning och ökad risk för föroreningar. Modellering av översvämningar i stadsmiljö har blivit allt viktigare med tanke på den potentiella risk som är associerad med hårda ytor. Med expanderande tätorter och en pågående klimatförändring är det viktigt för städer att han en fungerande dagvattenstrategi. De komplexa ytor och höjdskillnader som utgör en stadsmiljö måste vara inkluderade i den planering som görs i den urbana miljön.

Målet med denna studie var att skapa en metod för att lokalisera de ytor i en stadsmiljö som har en hög potential att översvämmas vid, eller under, en extrem nederbörd (>40 mm/dag). Detta gjordes med hjälp av GIS-baserad analys och fjärranalys genom att skapa en avrinningsmodell och en representation av de hårda ytor som förekommer i studieområdet. Resultaten illustrerar de områden som tros ha störst risk att översvämmas vid extrem nederbörd. Studieområdet är Lund, beläget i de södra delarna av Sverige. I studien används ett Orto-foto från 2010, erhållet från Lunds Kommun, som bas till analysen av hårda ytor. Detta resultat används sedan som input till avrinningsmodellen där avrinningsvolymer och avrinningsområden illustreras.

Resultaten indikerar att hårdgjorda ytor är en viktig komponent vid analys av avrinning i stadsmiljö. Stora anslutna hårda ytor har potential att producera stora mängder dagvatten om dem inte är dränerade. Resultaten visar även att vegetation har en stor potential att störa flödespassager och minska eller hindra översvämningar.

Nyckelord: Geografi, Naturgeografi, GIS, Fjärranalys, Geomatik, Hårdgjord yta, Extrem nederbörd, Stadsmiljö, Avrinning, Dagvatten, Lund

Acknowledgements

First of all, I would like to thank my supervisor for this study, Thomas Holst at the Department of Physical Geography and Ecosystem Science at Lund University, for his support and inspiration in writing this thesis. I would also like to thank Karin Larsson at the department for her initial help and inspiration to this study.

I would also like to express my gratitude at the Department of Surveying (Lantmäteriavdelningen), at Lund Municipality, for the permission to use their data as a part of this study. Special thanks are directed towards Tilda Brage and Ola Svensson at the department, for their time and willingness to help with this project.

Table of Content

1. Introduction

With ongoing climate change (Bhend and von Storch 2008; Giorgi and Lionello 2008; Vautard and Yiou 2009) and intensified urban development, the demands on a sustainable storm water management are increasing (Burns et al. 2012). Impervious surfaces, such as urban areas, reduce infiltration and increase runoff, with the potential to cause erosion and contribute to siltation and water pollution (Chen et al. 2009; Veracka 2013). To implement effective urban storm water management, proper consideration has to be given to the spatial variability of urban watershed characteristics (Meyer et al. 1993). Therefore it is important to have storm water regimes in mind when planning expansions of built up areas in an urban environments (Barbosa et al. 2012). It is important to plan for events that the drainage system cannot handle, such as extreme precipitation events. This could be done by dividing and delaying flow by e.g. altering the topography within specific areas (Barbosa et al. 2012) or by constructing "end-of-catchment" stormwater wetlands which could reduce peak flows (Burns et al. 2012). The topography is an important parameter in hydrologic and geomorphologic applications (Seibert and McGlynn 2007; Zhou et al. 2011). A key parameter in catchment topography is the flow distribution and how surface flow is routed within the area (Pilesjö et al. 1998; Zhou et al. 2011). The use of Digital Elevation Models (DEMs) has made it possible to estimate these parameters for each location over a surface (Pilesjö et al. 1998). The flow routing, or path, is calculated from the surface elevations. There have been several models created to describe surface elevations, such as triangulated irregular network (TIN), digital contour and hybrid structures (a grid with break-lines), and the most commonly used data representation for terrain analysis, the grid DEM (Zhou et al. 2011).

As stated above, the flow routing, or direction, can be derived from a DEM. From the flow direction, the up-stream flow accumulation can be modelled (Pilesjö et al. 1998). The flow accumulation can be used to predict the received flow at the pour point of a flow path. In a hypothetical environment, all precipitation that falls within an impervious area would become runoff and follow the flow paths described by the flow direction model. The runoff would then accumulate at the pour points. However, in reality infiltration and evapotranspiration would change the predicted surface runoff volumes (Chen et al. 2009).

Rapid urban growth during the last century and ongoing climate change have made it more difficult for urban areas to maintain effective storm water administration. Planners and decision makers must consider these changes to maintain or reach a proper storm water

management (Burns et al. 2012; Barbosa et al. 2012). Impervious surfaces increase runoff, risk of flooding and contribute to water pollution (Burns et al. 2012; Barbosa et al. 2012; Veracka 2013). In modern times, most developed cities treat rainfall within an urban area as waste. The reduced infiltration caused by impervious surfaces increases the risk of flooding. The water can also contain pollutants in the form of nutrients, oil and heavy metals (Barbosa et al. 2012; Burns et al. 2012).

In Sweden, two different directives exist to handle the excessive stormwater, “The Flooding Directive" (Översvämningsdirektivet) and “The Water Directive" (Vattendirektivet). The "Flooding Directive" was agreed upon by the EU as a way to decrease the negative effects of flooding and to protect human health and the environment (MSB 2011). The "Water Directive" exists to establish a protection for lakes, streams, coastal water and ground water (VA SYD 2013). Local strategies exist to uphold these directives and policies. In the report by VA SYD (2013), which is Lund Municipality's stormwater strategy, different examples are presented on how to change the present management approach to one where both the ecological and hydrological status within the municipality are improved.

1.1 Objectives of the study

Based on the information presented above, it is believed that with ongoing climate change, extreme precipitation events have increased both in frequency and magnitude, especially during summer months for the study area. Extreme events can be potentially problematic in urban areas (Chen et al. 2009; Barbosa et al. 2012). With large volumes of precipitation, it is also believed that impervious surfaces within an urban area would potentially cause high volumes of surface runoff, with possible flooding as a result (Chen et al. 2009). Areas with a proportionally high amount of impervious coverage are believed to be the most prone to accumulate large volumes of runoff.

The primary aim of this study was to create a method to locate and map urban areas with large surface water runoff volumes in the occurrence of an extreme storm event. The study also investigated which of these areas have the highest potential to flood in the event of an extreme storm. This was done by creating a runoff model based on an impervious surface analysis conducted on a high resolution Ortho-image, in combination with a terrain analysis of a DEM in a GIS (Geographical Information System) environment. In addition, precipitation data for the study area was investigated and used as input for the runoff model. Vector data was used as a complement in locating buildings within the urban area. Two simplifications were made

in this project, where water conveyed by the sewer network was excluded and buildings were considered as pervious ground.

The objective of this study was to answer the following research questions:

- Has precipitation (seasonal and daily) increased between 1961-2012 and what are the magnitudes of the most extreme rainfall events during this time?
- Are impervious surfaces an important factor when analysing runoff in an urban environment and is it the most important factor to consider when conducting a runoff analysis in an urban setting?
- Where are the areas with the highest runoff volumes located within the study area and are they similar in surface composition?
- Are the areas with largest runoff volumes thought to be those most prone to flooding?

1.2 Study area

The study area is located in Scania (Skåne) in southern Sweden in the municipality of Lund, see **Figure 1**. Lund municipality has a total area of 439.9 km^2, where Lund city covers 2775.03 ha (27.75 km^2) (SCB 2014). The extent of the study area is 40.08 km^2 and stretches a short distance outside of the city limits. Lund municipality had a population of 114 654 in 2010, whereof 82 800 lived in urban Lund. The urban population has grew with 9% between 2005 and 2010 (SCB 2014).

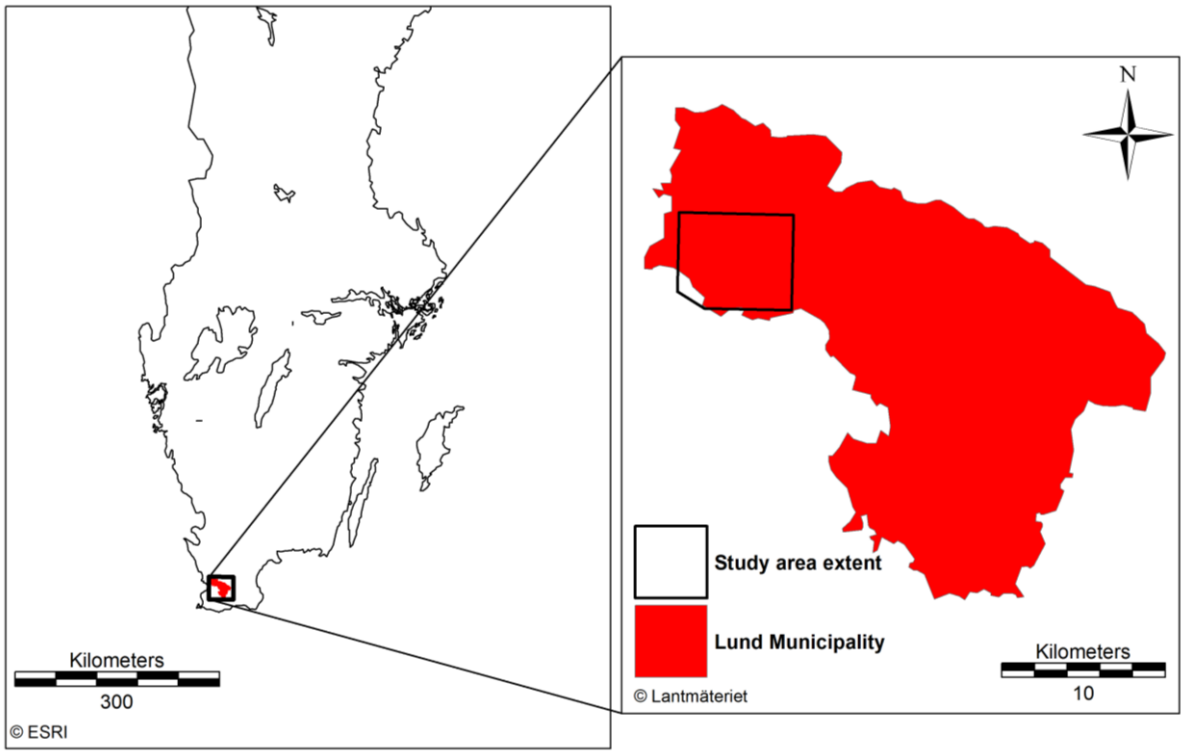

Figure 1 *On the left, Lund municipality inlaid in a map illustrating the southern parts of Sweden. On the right, Lund municipality with inlaid study area extent. The extent of Sweden is downloaded from ESRI (2014), municipality border downloaded from Lantmäteriet (2014).*

The municipality is dominated by agricultural fields and has undulating terrain (Linderson 2002; Achberger et al. 2003). Scania climate is classified as warm temperate, fully humid with warm summers (Cfa) according to the Köppen classification done by Kottek et al. (2006). The region is affected by cyclonic activity year round, with maximum activity during the winter. The precipitation is mainly caused by cyclonic activity, although during summer convective processes contribute significantly to precipitation volumes (Achberger et al. 2003). The mean annual precipitation for Lund from 1961 through 2011 was 670 mm (Bengtsson and Rana 2014).

Much of the runoff from urban Lund is directed to the south-western parts of the study area, where Lund's treatment plant is located alongside Höje Å. This small stream later drains into the sea to the west (VA SYD 2013).

2. Theoretical Background

2.1 GIS and remote sensing

Geographical Information Systems are computer driven programs that handle information referenced by a geographical location. They are able to handle both locational data and attribute data. This enables the user to both produce maps and to conduct analysis of the data within the GIS program (Lillesand et al. 2008).

Remotely sensed data is data acquired by a device not in contact with the object, area or phenomenon that are being investigated. The data is collected by sensors attached to e.g. airplanes or satellites and can be of many forms, including measurements of reflected electromagnetic energy. This data can be illustrated using images depicting vegetation, clouds and other earth resources. To analyse the information contained in these images, a GIS program can be used. The product of this can be either a map, illustrating e.g. forest cover, or an analysis about e.g. seasonal change in temperature (Lillesand et al. 2008).

The usage of GIS and remote sensing plays a major part in this study. The land cover classification was performed using remote sensing in GIS. The result was then analysed and used as input to produce a result from the runoff model, all done in a GIS environment.

2.2 Digital Elevation Model

DEMs are often of the type *Regular Square Grids* (RSGs) which are a 3D representation of the terrain in a digital format. It has a finite set of points spaced regularly in an x and y environment (Floriani and Magillo 2009). Large and accurate DEMs are usually acquired through the use of remote sensing, either from aerial or satellite sensors. In the case of very large DEMs the storage and processing can be inefficient. Generalization of the DEM is often performed to reduce storage size and improve processing times. This often comes at the cost of accuracy (Floriani and Magillo 2009).

Because of the RSG structure, the DEM is an approximation of the real-world continuous surface using regular spaced samples. Terrain analysis performed on a DEM is naturally affected by the assumptions used in the creation of the DEM model (Zhou et al. 2011). As stated in the introduction of this study, the usage of a DEM is popular when conducting terrain analysis. The most important information derived from a DEM in this study is the flow routing, or flow direction, within the study area. Flows will follow these paths until they reach a sink or the edge of the study area (Holmgren 1994). The flow direction is controlled by the slope, which also influences the subsurface flow (Pilesjö et al. 1998; Zhou et al. 2011).

Several different flow direction algorithms exist for this purpose (Holmgren 1994; Pilesjö et al. 1998; Seibert and McGlynn 2007; Zhou et al. 2011). What is generally called an Eight-Direction (D8) (O'Callaghan and Mark 1984; Jenson and Domingue 1988) or a Single Flow Direction (SFD) algorithm was used in this study. The SFD will determine flow in one of eight possible directions from each cell (to one of the eight neighbouring cells) (Jenson and Domingue 1988) and will not allow flow divergence (Zhou et al. 2011).

From the flow direction, flow accumulation can be derived (Pilesjö et al. 1998) and used to model the upslope accumulation area (Seibert and McGlynn 2007).

2.3 Classification scheme

When working on land cover classifications and mapping, it is important that there is a classification scheme to be used throughout the procedure to separate different land covers. In many cases an existing scheme could be used, but in other situations the scheme could be decided based on the objective or limitations of the project (Congalton 1991). The scheme should work in a way that all areas that are classified should only be classified as one category and that all areas within the study area should be classified (Congalton 1991).

It is also an advantage if the scheme is hierarchical, meaning that classes could be collapsed to create more general categories (Congalton 1991). A highly detailed scheme will increase the time needed to conduct an accuracy assessment (Congalton and Green 1999).

2.4 Field sampling

To accurately describe land cover classes, a field sampling could be needed (Congalton 1991). To use a remotely sensed image as a reference for itself would create an assumption that the interpretation of the image is correct (Congalton 1991). If results from image interpretation were to be used as reference data, errors would be blamed on the digital classification and would lower the classification accuracy (Congalton 1991). For a classification to be performed well, at least 50 points for each class are needed (Congalton and Green 1999). These samples will serve two purposes in the classification process, first as training sites for the classification, and second as reference samples for an accuracy assessment (Thomas et al. 2003). The size of the samples is also important to achieve a high accuracy of classification. According to McCoy (2005), the sample should be at least the size of a ground pixel, preferably larger.

When collecting field samples the possible locational error caused by the Global Positioning System (GPS) must be considered. The amount of satellites connected to the GPS receiver, as

well as the time used collecting the sample, influences the accuracy of the position (McCoy 2005). This is important to take into consideration when deciding on a sample area for each location.

The method of collecting samples is also an important factor in remote sensing. Random sampling has good statistical validity, but can be difficult to use in practice, since samples can be hard to access in the field. A combination of random and systematic sampling could be a good alternative to achieve a sound result (Congalton and Green 1999).

2.5 Accuracy assessment

Accuracy assessment of a land cover classification is often required for evaluating the quality of the classification or for identifying a suitable classification method. This can be done by comparing the results from different methods performed within the area (Lu et al. 2011). Accuracy in remote sensing is often expressed as a degree of "correctness" of the map classification. A thematic map (classification map) can be considered accurate if the result is an unbiased representation of the area it describes (Foody 2002). It is important to evaluate the accuracy of a classification, especially if the result is to be used in a decision making process (Congalton and Green 1999). There are different ways to assess the accuracy. One way is to use a quantitative approach, where mapped data is compared against a set of reference data where the reference data is expected to be accurate (Congalton and Green 1999).

The most used and preferred quantitative method is the error matrix approach (Congalton 1991; Foody 2002; Lu et al. 2011). The elements of an error matrix include overall accuracy (OA), producer's accuracy (PA), user's accuracy (UA) and the kappa coefficient (KC) (Lu et al. 2011). The importance of a fair accuracy assessment can be found in Congalton (1991).

The producer’s accuracy (error of omission) is calculated by taking the total number of correctly classified samples in a category, and dividing this by the total number of samples for that category. The total number of samples for each category is derived from the reference data (column total) (Congalton 1991; Richards and Jia 2006).This accuracy will represent the probability of a reference pixel being correctly classified (Congalton 1991). It is a measure of how well a certain area can be correctly classified (Congalton 1991; Richards and Jia 2006).

To calculate the user's accuracy (error of commission), the total number of correct samples (from reference data) in a category is divided by the total number of samples that were

classified as that category. This measurement could be said to reflect the reliability, or the probability, that a classified pixel or area in the map actually represents the class in which it is categorised (Congalton 1991).

The Kappa coefficient, or Cohen's kappa, is another way of evaluating the accuracy of a classification and is used as a measure of how well the remotely sensed classification agrees with the reference data (Congalton and Green 1999). The Kappa value can be less than or equal to 1, where 1 suggests a perfect agreement and 0 would correspond to a random classification. The Kappa value can also be negative. When the Kappa value is negative, it suggests that the accuracy of the classification is less than would be expected by chance (Congalton and Green 1999).

Kappa is calculated as:

$$K = N\sum_{i=1}^{r}\chi_{ii} - \sum_{i=1}^{r}(x_{i+} \times x_{+i}) \Big/ N^2 - \sum_{i=1}^{r}(x_{i+} \times x_{+1}) \qquad \text{(Eq. 1)}$$

where N is total number of observations in the matrix, r is the number of rows, x_{ii} is the total number of observations in row i and column i, x_{i+} and x_{+i} are the marginal totals of row i and column i in that order (Congalton 1991).

2.6 Runoff

Overland flow within a catchment occurs when rainfall or snowmelt exceeds the infiltration capacity of soil or when the surface is incapable of further infiltration due to saturation (Hornberger 1998). The infiltration rate, the rate at which water infiltrates into soil, exerts major control over the surface water flow (Morgan 2005). When the soil is saturated, the excess water will contribute to surface flow. This saturation point is known as the infiltration capacity or terminal infiltration rate (Hornberger 1998; Morgan 2005).

The runoff, or flow, is often referred to as Hortonian overland flow after the American hydrologist Robert Horton (Hornberger 1998). The infiltration of soil is dependent on the soils properties. Vegetation and soil roughness strongly influence these properties (Hornberger 1998). Both above-ground vegetation and below-ground vegetation provide roots that keep soil highly porous and permeable. Vegetated areas often provide low to no runoff, based on these properties.

Urban environments, which are often composed of large impervious surfaces, are characterised by reduced infiltration capacity and accelerated runoff (Chen et al. 2009). Accumulation of runoff in these environments causes flooding unrelated to the flood-plain environment. Extreme events, which was analysed in this study, have the potential to cause flash floods when drainage is incapable of relieving the area of excess water (Chen et al. 2009).

3. Data and method

This study consists of several parts. The first sections (Ortho-image, Terrain model, Vector data and Precipitation) describe the data and the pre-processing performed before the analysis. The following sections will describe the GIS analysis and the precipitation analysis. All information regarding the Ortho-image and the DEM is taken from data description written by BLOM Sweden AB. This report contains information about the equipment used in gathering the remotely sensed data, as well as information about the pre-processing done before delivery. BLOM Sweden AB performed the tasks of capturing and delivering the Ortho-image and the DEM on behalf of the municipality of Lund. The rights for the Ortho-images, DEM and the vector data belong to the municipality of Lund and were used with permission.

The software used for pre-processing and GIS analysis are ArcGIS 10.0, IDRISI Selva, MATLAB R2012 and Microsoft Excel.

3.1 Ortho-image

To achieve an accurate representation of the impervious surfaces in urban Lund, a high resolution image was preferred. A multispectral Ortho-image with the resolution of 0.25 x 0.25 meters was chosen as input for the process of creating the impervious surface map. The use of a high resolution image reduce problems inherent in lower resolution imagery, such as mixed pixels (Lu et al. 2011) but can increase the "salt and pepper" effect after classifications (Lu et al. 2011). This effect is created when a small number of clustered pixels are classified different than the surrounding pixels.

The Ortho-image is a composite created from images taken during the time period of 2010-06-02 to 2010-06-06 and consists of three bands. Band 1 represents the Near Infrared spectrum (NIR, 750-900 nm), Band 2 represents the Red spectrum (630-680 nm) and Band 3 represents the Green spectrum (520-590 nm). These three bands constitute what is called a FCC (False Colour Composite). The images were captured with the sensor Vexcel UltraCam XP, at an altitude of 4200 meters with a 60% (65% in urban areas) overlap. Pre-processing performed by BLOM Sweden AB include mosaicing and colour and contrast calibration. The image was delivered in TIFF-format with the coordinate system SWEREF 99 1330.

3.2 Terrain model

Another important part of the study is the terrain model. A DEM with high accuracy and high resolution was needed to give a good result in the runoff model. The terrain model used in this study was a DEM with a 2 x 2 meter resolution in RSG-format, constructed by BLOM

Sweden AB. The DEM has, before acquisition, had large topographical errors corrected and was supplemented with break-lines at certain locations such as bridges etc. The terrain model has been compared to reference points on the ground to ensure its accuracy. The root-mean-square error was reported as 0.11 m.

In **Figure 2**, the study area is illustrated by the DEM together with the vector buildings layer used in the study. The dark area in the south west corner is the treatment plant of Lund and Höje Å, a stream that flows past the southern border of the built up area of Lund.

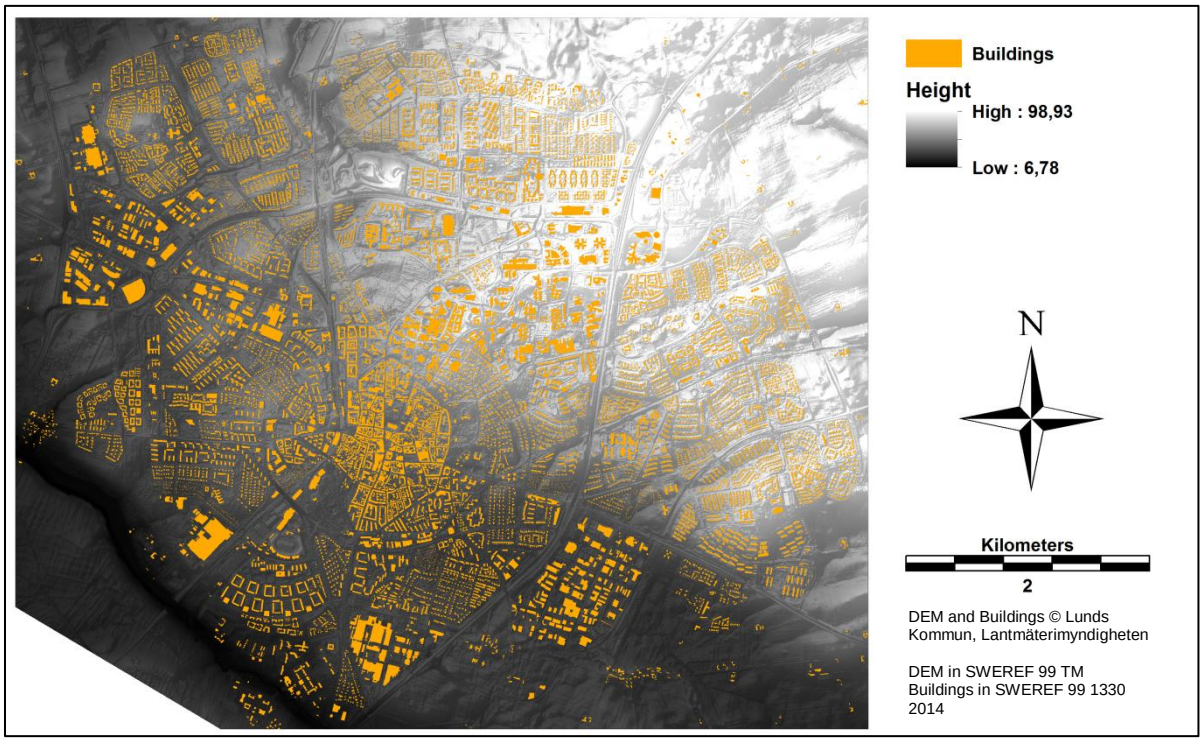

Figure 2 *The terrain of the study area illustrated by the DEM used in the study. Overlaid polygons represent buildings within the study area. Data used with permission from Lund Municipality.*

3.3 Vector Data

To complement the impervious surface analysis, a vector layer containing the locations of all buildings within the urban area of Lund was used (see **Figure 2**). The data contains polygons covering all buildings within the study area that are collected and updated by the municipality of Lund. The data was used to extract the area of the buildings for the impervious surface analysis, as described later in the text. The data was used with permission from Lund Municipality.

3.4 Precipitation

Precipitation data was downloaded from the Swedish Meteorological and Hydrological Institute (SMHI) through their web service "Öppna data" (http://opendata-download-

metobs.smhi.se/explore/). The data covered the time period of 1961-01-01 through 2012-12-31 at daily resolution. A higher temporal resolution was not available for the complete time period. All data was available in the public domain.

The precipitation records from Lund (climate station number 53430) were gathered from three different locations, where the first two only differ in height. The first two locations was at 55.71; 13.20 (latitude/longitude in WGS 84), which lies in the central eastern parts of the urban area. Between 1961 and 1974, the height (above sea level) was 73 meters, the station was then moved nearby to a lower altitude of 50 meters above sea level. In 1992, the location of the climate station was changed to a more secluded part of the town, outside of the inner city. The new location is at 55.70; 13.23 (latitude/longitude in WGS 84), which is in the south eastern outskirts of Lund, at the city's fire station. Prior to downloading, the record had been checked and corrected by SMHI and likely includes entries that have been interpolated to cover missing values.

The time series was divided into two different time periods, one covering the current climate normal period (1961-1990) and one for the remaining years (1990-2012). This was done to locate different maximum values for comparison in the runoff model.

The precipitation data was analysed to find means and maximums on a daily, multi-day (3-day), monthly and yearly basis. Extreme events (>40 mm/day) were also investigated.

An estimation of future precipitation was also analysed. This was done by using modelled data downloaded from SMHI (http://www.smhi.se/klimatdata/Framtidens-klimat/Klimatscenarier/2.2252/2.2271). The data is delivered as an estimated yearly (or seasonal) precipitation change. It contains estimations from 9 different climate models attuned to the RCP 8.5 scenario (Representative Concentration Pathway) (Kjellström 2009).

The RCP 8.5 scenario assumes high population with relatively slow income growth and modest rates of technological change. It predicts low energy intensity improvements which lead to high energy demand and high GHG (Greenhouse Gas) emissions. In comparison to other RCPs, the RCP 8.5 is the pathway with the highest greenhouse gas emissions (Riahi et al. 2011). The RCP 8.5 scenario was chosen to portray a large difference compared to the current climate normal period.

The scenario data (RCP 8.5) was then compared to the measured data from SMHI. The time period 2061-2091 was selected in the scenario data, and the average precipitation change (in

percent) over all 9 models was calculated. The analysis also included the predicted maximum increase and decrease (in percent) for the same time period. The result was the percentage change of precipitation compared to the measured precipitation for the time period 1961-1990.

3.5 GIS analysis

3.5.1 Impervious surface analysis

To extract and classify areas as impervious surfaces, a land cover classification was needed. In the land cover classification, a set of categories were decided upon to distinguish between impervious surfaces and pervious surfaces. To accurately perform the land cover classification, a field sampling for training sites and references points was needed. To conduct the impervious surface analysis, a set of land cover classes had to be decided, see **Table 1**, and a classification scheme defined, see **Table 2**.

Table 1 *The categories for the land cover classification. Tier 2 could be collapsed into tier 1, where bare soil, vegetation and water all would be described as pervious surfaces.*

Categories (tier 1)	Categories (tier 2)
Impervious surfaces	Impervious surfaces
Pervious surfaces	Bare soil Vegetation Water

The categories were designed with the intent to be collapsed into two main classes after classification, impervious surfaces and pervious surfaces. Bare soil was included in the field sampling and classification process due to a high presence of this class in the Ortho-image.

When testing the classification described above, it was realised that water as a class would be hard to correctly classify due to a high amount of shadow in the urban areas. The decision was made to use a different approach to classify areas covered with water after the land cover classification was done, and not to collect samples of locations of water in the field.

The field sample collection was not performed in a strictly random format. Limited time and accessibility to locations within the built up area made that impossible to achieve. The samples were collected in a purposeful manner that was deemed representative of the class they described. Although the format was non-random, the samples had to be spatially representative within the study area. The classification scheme is shown in **Table 2**.

Table 2 *The classification scheme for the land cover classification.*

Classification scheme
• Each sample should be homogenous (3 meters in diameter, 12 pixels) • The minimum distance to the next class must be 5 meters (20 pixels) • The samples have to be good representations of the class they describe • Samples have to include variations within each class (trees and grass in vegetation etc.) • Samples have to be spatially representative within the study area

The collection of samples within the urban area was limited by availability. Samples had to be taken in publicly accessible areas and not in private gardens etc. As mentioned in **Table 2**, each sample had to be homogenous and 3 meters in diameter (12 pixels). This was based on information given by McCoy (2005), that a sample should be at least the size of a ground pixel (0.25 meter for this study). To further secure the integrity of the samples, a restriction was set that the location of each sample had to be no less than 5 meters from a different class.

The sampling was performed with a handheld GPS receiver using WGS84 as the coordinate system. The samples were then imported into GIS and transformed into SWEREF 99 1330 to match the coordinate system of the Ortho-image. The number of samples for each class is presented in **Table 3**.

According to Congalton and Green (1999) at least 50 points in each class are needed for the classification to be statistically sound. For bare soil, this proved difficult to achieve. The number of locations within the urban area with bare soil was limited, and sampling of points too close to each other and within the same area would not fulfil the spatial distribution requirement.

Table 3 *Number of samples collected for each class in the field sampling.*

Category	**Number of samples**
Impervious surface	54
Bare soil	7
Vegetation	53

After importing the samples into GIS, they were split into two groups, training sites and reference points. The samples selected as training sites were to be used as input for the land cover classification and the remaining points were to be used as reference samples in the accuracy assessment. The training samples had a buffer zone of 6 meter in diameter created at each location. These new areas were used to create the spectral signature for each class.

To validate the accuracy of the collected samples, a spectral signature comparison was performed. This included a signature comparison of the minimum, maximum and mean

values of the spectral signals. Scatterplots comparing the signal between two bands at a time was also used. The tests revealed similarities between classes and the risk of misclassification between classes. The samples were also compared to training sites selected from the Ortho-image to validate the accuracy of the samples. These training sites were chosen using visual inspection and interpretation and were not based on field observations.

The land cover classification was performed using maximum likelihood classification, where pixels are assigned to the most probable class based on the information given by the signatures from the training sites (Richards and Jia 2006; Li et al. 2010). The result of the land cover classification was then assessed using an error matrix and visual inspection. The result was compared to classifications done using the manually selected training sites from the Ortho-image previously mentioned.

Water was added to the land cover classification based on the spectral characteristics found only in the near infrared band. The information was used to reclassify pixels deemed to be water and change these areas to water in the land cover classification.

Prior to use in the runoff model, the result from the land cover classification was collapsed in accordance with the hierarchy described in **Table 1**, to create two classes, impervious surfaces and pervious surfaces.

3.5.2 Runoff model

The main goal of the runoff model was to estimate the cumulative rainfall excess that accumulates in depressions within the study area. The rainfall excess, or surface runoff (R) is the rainfall that is not infiltrated and is measured in cubic meters (**Equation. 2**), P is the cumulative rainfall volume in cubic meters and F is the cumulative infiltration in cubic meters (Chen et al. 2009).

$$R = P - F \quad \text{(Eq. 2)}$$

The model was a simplified version of the one used by Chen et al. (2009). There were certain assumptions made to simplify the model. Evaporation was excluded from the calculations, based on its relatively low influence on flooding events (Chen et al. 2009). Water conveyed by the sewer network in the urban area was also excluded in this study due to time limitations regarding proper implementation and limited information regarding locations of drains.

The infiltration (F) was estimated using a modified Green-Ampt model (Green and Ampt 1911) used by Chen et al. (2009). It is a simplified representation of the infiltration process of vertical flow. The Green-Ampt model was used to estimate the influence of land use on the infiltration by applying an adjustment index for impervious surfaces, φ. φ is calculated based on the percentage impervious surface area (μ) in each cell in the study area (**Equation 3**) (Chen et al. 2009).

$$\varphi = 1 - \mu \quad \text{(Eq. 3)}$$

The percentage of impervious area (μ) in each cell was estimated through the aggregation of the land cover classification result. The land cover map had a resolution of 0.25 m but was aggregated (by a factor of 8) to match the DEM's 2 meter resolution. A raster was created with the same extent and resolution as the impervious surface raster where all cells had a value of 1. This raster was then subtracted with the impervious surface raster. This resulted in the adjustment index (φ), which was used to adjust the infiltration over impervious surfaces (Chen et al. 2009). Buildings were extracted from the impervious surfaces and were considered to be pervious. This decision was based on the hypothesis that most of the water collected by rooftops was directly routed through drains and away from overland flow, and thus not of interest to this study.

The volume of cumulative infiltration (F) was an estimation based on the soil types in the study area. This have been estimated based on a soil map from SGU (2014). The dominant soil type for the study area was determined to be clay till, with small amounts of postglacial clay and glaciofluvial sediments.

The infiltration rate is determined by the soil type and the soil moisture (Hornberger 1998). The infiltration of dry soil is initially very high but decreases over time when the water moistens the surface layers (Hornberger 1998). Since the dominant soil type in the study area is composed of clay material or material with high amounts of clay, the assumption was made to use the infiltration rate and infiltration capacity of clay soil. The infiltration capacity of clay was estimated to be around 6.25 mm/h for saturated soil using values from Morgan (2005), see **Figure 3**.

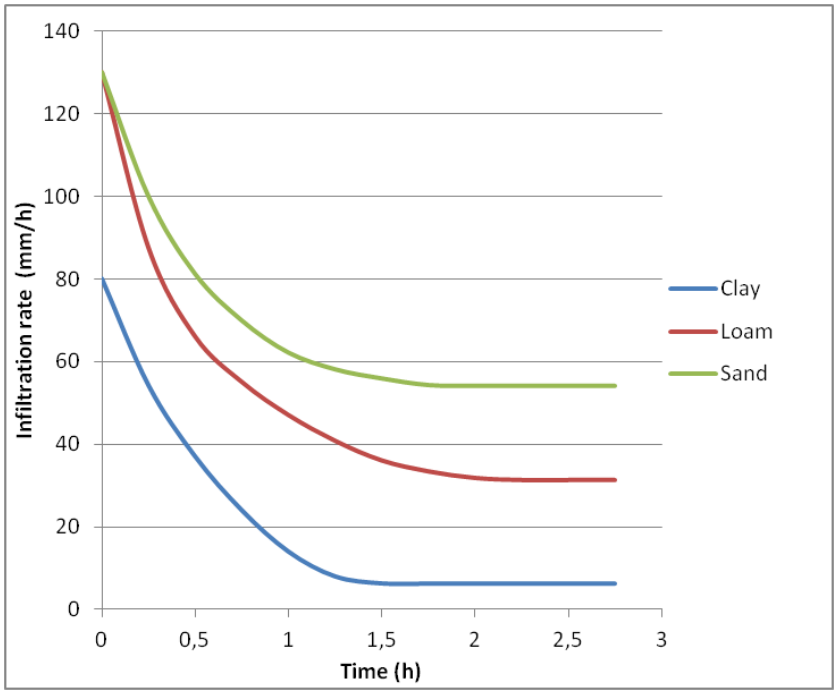

Figure 3 *Estimated infiltration rates for three different soils. The graph is adapted after Morgan (2005).*

The cumulative infiltration (F) is the infiltration over time for each cell. The adjusted infiltration (q) was computed from F in accordance with **Eq. 4** (Chen et al. 2009).

$$q = F * \varphi \qquad \text{(Eq. 4)}$$

Three different time scenarios were used, see **Table 4**. The first scenario represents the cumulative infiltration volume after a 3 hour time period. The second entry displays the infiltration volume after a 24 h time period, and the last scenario displays the infiltration volume over a 3-day (72 hours) time period. The values presented in the table represent the potential infiltration for an area with pervious coverage.

Table 4 *The potential cumulative infiltration volume (F) for three different time scenarios. The cumulative volume is shown in cubic meters (m^3) and included the ramp up infiltration until the infiltration capacity was reached (terminal rate). The volume is shown for 1 m^2.*

Time period (h)	Cumulative infiltration volume (m^3)
3	0.0637
24	0.195
72	0.495

The adjusted infiltration (q) was used to compute the runoff by replacing F in **Eq. 2** so that it can be rewritten as **Eq. 5** (Chen et al. 2009).

$$R = P - q \quad \text{(Eq. 5)}$$

The result from **Eq. 5** is used as the precipitation input in the runoff model as a raster with 2 x 2 meters resolution.

3.5.3 Flow direction and flow accumulation

The first part of determining the runoff volume was to calculate the flow directions for each cell based on the DEM. This was done using the built in flow direction tool in ArcGIS. This tool uses an algorithm based on work by Jenson and Domingue (1988). The algorithm was a SFD (D8), which is described previously (**Chapter 2.2**).

The result of the flow direction model and the runoff model was used to determine the distribution of runoff within the study area. This was done by calculating the flow accumulation, where each cell is assigned a value that is equal to the number of cells that flow to it (Jenson and Domingue 1988).

The runoff was used as a weight in the flow accumulation calculation. The flow accumulation model produced a result based on the flow direction input, and the runoff was then multiplied with this result to create a raster with volume of the accumulated flow. The result displayed all flow paths within the study area. Each cell with a value represented the accumulated upslope flow for that cell.

3.5.4 Catchment delineation

DEMs can contain depressions, areas where the flow routing will be hindered or stopped (Jenson and Domingue 1988). When conducting a flow direction analysis to identify streams within a study area, these depressions are normally flattened by a fill function so that the DEM is "depressionless" (Jenson and Domingue 1988). In this study, these areas were of interest and were therefore left in the DEM.

To localise areas with high amounts of accumulated flow, a watershed analysis was performed. This was done by determining a threshold value based on the flow accumulation result from the 1961-1990, 3-hour scenario. This threshold was used for all calculations covering the 24-hour span. For the 72-hour scenarios, a second threshold was determined

from the 1961-1990 time period. The thresholds represent the 90th-percentile of the flow accumulation result.

Watersheds were delineated using the built in tool in ArcGIS. The tool required the flow direction previously described, and location of pour points. These pour points are represented by the threshold value described above and are the last receiving cell for each watershed or catchment. The tool established the upslope contributing area for each pour point, thus creating a result with watersheds within the study area.

Watersheds not in the vicinity of the main urban areas of Lund were then excluded from the continued analysis. The vicinity was established from visual interpretation of the watershed result in comparison with the Ortho-image. Watersheds consisting of exclusively fields were excluded from further analysis.

Further restriction in the selection of watersheds was applied by a secondary limitation. Watersheds had to contain 10 or more connected cells, all with a runoff volume above the threshold. This restriction was applied to exclude very small areas from the result. The number of connected cells for each catchment is also used to represent flow path length.

The watersheds produced from these operations will be denoted as catchments from this point on.

An index, see **Equation. 6**, was created for each catchment:

$$Runoff\ volume\ /\ Area\ of\ catchment\ =\ Runoff\ Index \quad \text{(Eq. 6)}$$

where $Runoff\ Volume$ is the derived runoff for each catchment (in m^3) and time scenario, and the $Area\ of\ catchment$ is each catchment's area (in m^2). The runoff index represents the height of the water level for each catchment if accumulated runoff was spread evenly within each catchment.

4. Results

4.1 Precipitation

The mean annual precipitation for Lund between 1961-1990 was at 658.4 mm and 671 mm for the whole time period of 1961-2012. There was a very slight increase of the mean annual precipitation over the whole time series, and comparing 1961-1990 with 1991-2012, the increase was 1.7%.

The yearly distribution of precipitation during the current normal climate period is shown in **Figure 4**. The highest monthly precipitation generally occurred during July with a mean of 68.8 mm. The autumn precipitation values are generally close to the summer values. November had the second highest precipitation mean with 67.4 mm. June had generally a low amount (53.9 mm) of precipitation compared to the following months.

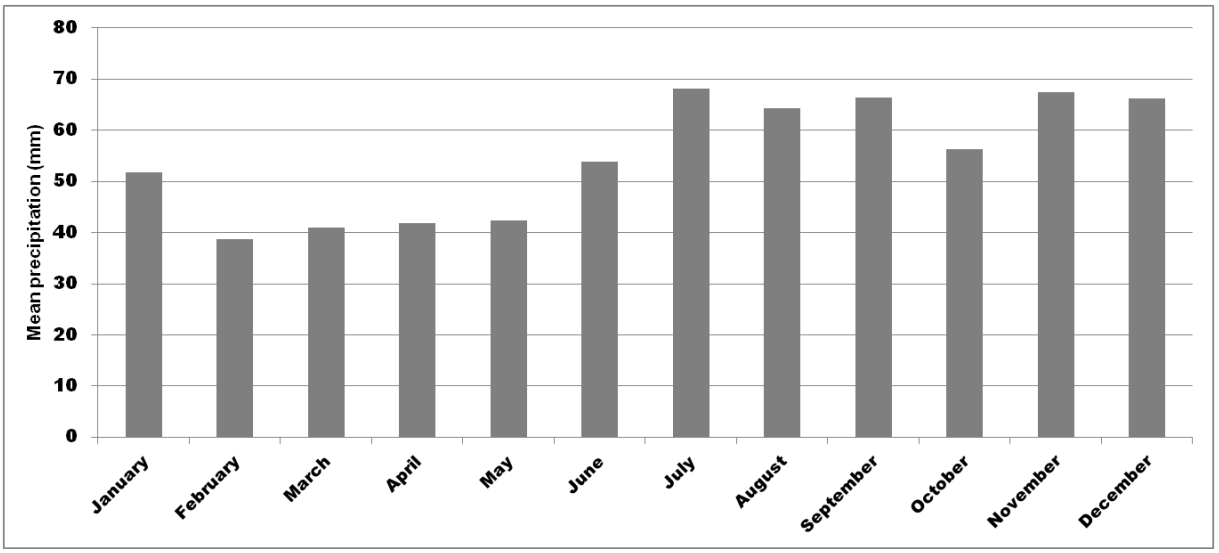

Figure 4 *The yearly precipitation (mean) for each month during the current normal climate period (1961-1990) for Lund (climate station number 53430. As seen, July has generally the highest precipitation during a year. Both summer and autumn precipitation values are similar.*

The maximum precipitation values for Lund analysed from the SMHI-data are shown in **Table 5**. The maximum precipitation for one day in the current normal climate period was 56.3mm. For the period after 1990, the highest precipitation amount for a single day is 58.2mm. Looking at a 3-days period, the highest precipitation for the time period 1961-1990 was 66.7mm and 94.7mm for the period after 1990.

Table 5 *The maximum daily precipitation in Lund for one day over the time periods of 1961-1990 and 1991-2012 in mm. The three-day maximum represent three consecutive days of precipitation, in mm.*

Scenario	Date	Precipitation (mm)
Max 1-Day 1961-1990	June 17th 1963	56.3
Max 1-Day 1991-2012	July 6th 2007	58.2
Max 3-Day 1961-1990	June 17th-19th 1963	66.7
Max 3-Day 1991-2012	July 5th-7th 2007	94.7

For an event to be considered extreme, the precipitation must exceed 40 mm/day (Bengtsson and Rana 2014). Looking at a yearly basis, as shown in **Figure 5**, there were 5 events such as this during 1961-1990 and 6 events during 1991-2012; a total of 11 events during the whole time period. Both the years 2000 and 2007 had two events exceeding 40mm/day.

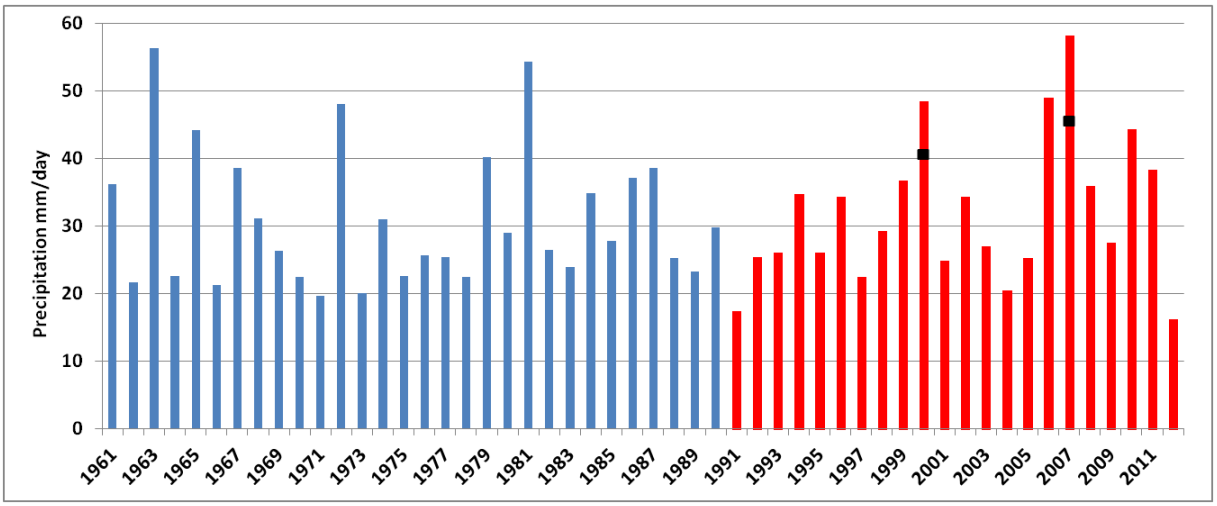

Figure 5 *Yearly maximum precipitation per day for Lund. The time period between 1961-1990 is marked in blue and the time period 1991-2012 is marked in red. Extreme events represent precipitation above 40mm/day. Two years (2000 and 2007) had 2 extreme events occurring; the volumes of these are marked with a black box.*

The maximum precipitation event for 1961-1990 occurred in June, while the maximum for 1991-2012 occurred in July. The daily maximum was part of the 3-day maxima for both of the time periods. Since the maximum precipitation occurred during the summer period, the main focus of the precipitation analysis was aimed at the summer months June, July and August.

Figure 6 displays the maximum daily summer precipitation for Lund from 1961-2012. The time period 1961-1990 is shown in blue to indicate the current normal climate period. The time period 1991-2012 is shown in red.

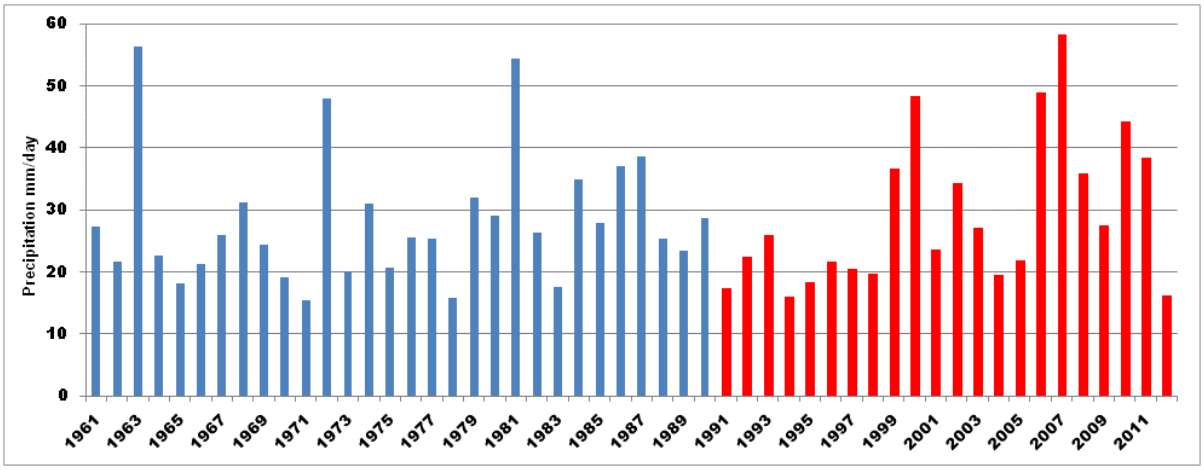

Figure 6 *The daily maximum summer precipitation for Lund during the summer months (June, July and August) from 1961-2012. The years 1961-1990 are shown in blue, and the years 1991-2012 are shown in red.*

Over the whole time period, there were six maxima with values close to, or over 50 mm precipitation for one day. During the first 20 years there were 3 events evenly spaced with a 10-year interval. This seems to change during the later part of the time period. The mean maximum over the whole time period was at 28.59 mm. For the first 30 years, the mean maximum is 28.15mm, while the last 22 years have a mean maximum of 29.2 mm. The average total summer precipitation for Lund is at 186.4 mm/ year.

Analysis of the future precipitation with scenario RCP 8.5 (**Table 6**) predicts an increase of 17.9 % for the yearly precipitation (2061-2090) compared to 1961-1990, over all models. The average yearly maximum increase for this time period is at 44.4 %, while the predicted maximum decrease is at 5.5 %. This resulted in a spread of over 49.9 percentage points. The average maximum increase and decrease is calculated from the largest change on a yearly basis, over the whole time period.

Table 6 *Predicted change in yearly precipitation for Scania with the RCP 8.5 model scenario for 2061-2090 compared to 1961-1990. The results were composited from 9 different climate models and the presented change is a mean over all the models. The average maximum increase and decrease represent values from single models for each year (largest change for each year). The spread is the difference between the increase and decrease predictions.*

RCP 8.5 2061-2090 (yearly)	Percent change (%)
Average change (all models)	17.9
Average maximum increase	44.4
Average maximum decrease	-5.5
Spread	49.9 percentage points

An analysis of the change in summer precipitation was also performed in the same way as for the yearly predictions. The results show an average increase of summer precipitation for Scania of 11.4 %. In this analysis, the spread between the increase and decrease is larger than for the whole year. The predicted maximum increase is 87.1 %, which is almost double the

prediction for the yearly change. The maximum decrease for the same scenario predicts a decrease of -44.2 %. The spread for summer precipitation is 131.3 percentage points.

Table 7 *The predicted change in summer precipitation with the RCP 8.5 model scenario compared to observations from the summer season between 1961-1990 for Scania. The result is composited from 9 different climate models and the presented change is a mean over all models. The average maximum increase and decrease represent values from single models for each year. The spread is the difference between the increase and decrease predictions.*

RCP 8.5 2061-2090 (summer)	Percentage change (%)
Average change (all models)	11.4
Average maximum increase	87.1
Average maximum decrease	-44.2
Spread	131.3 percentage points

4.2 Impervious surface analysis

By testing an unsupervised classification (clustering, based on Richards (1986)) and a supervised classification (maximum likelihood, based on Richards (1986)) it was, based on a combination of visual inspection and accuracy assessment, decided that a supervised classification produced the best result.

4.2.1 Land cover classification

Figure 7 shows the signature comparison chart for the three different signatures created based on the field samples (see **Chapter 3.5.1**). It shows the mean value (pixel value) for each class, as well as the minimum and maximum spread within the class for the three bands used in the classification. The most important pieces of information gathered from this graph are the similarities or dissimilarities between impervious surfaces compared to bare soil and vegetation. As seen, vegetation is clearly dissimilar in the spectral signature (over all bands) when compared to impervious surfaces, while bare soil has many similarities (in all bands) with impervious surfaces.

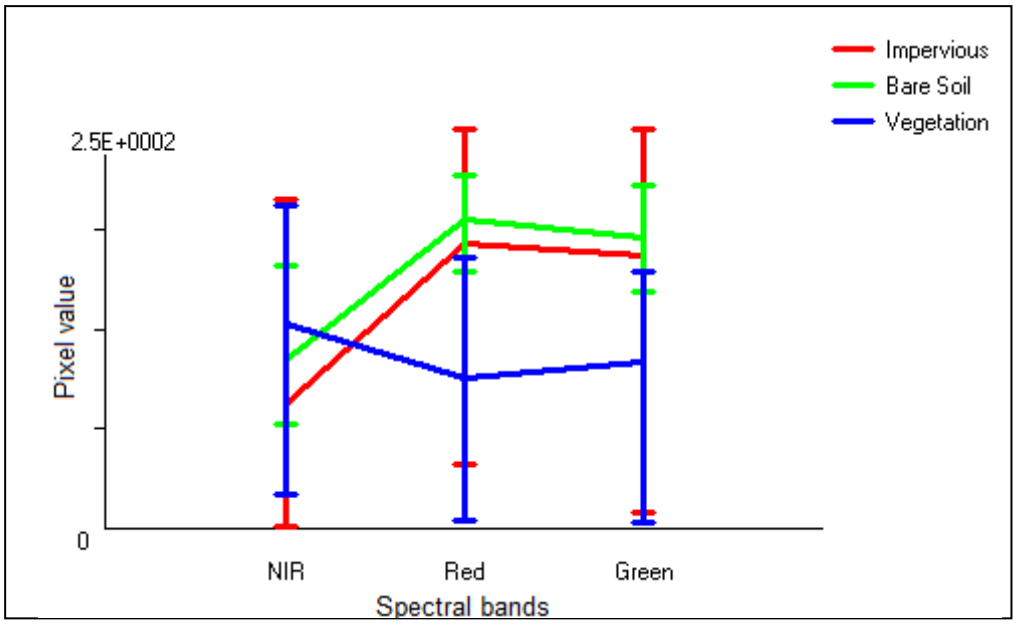

Figure 7 *Signature Comparison Chart for the three different classes in the maximum likelihood classification. It shows the mean value (pixel value), maximum and minimum value within each class separated by the three spectral bands used (NIR, (750-900 nm), Red (630-680 nm) and Green (520-590 nm)).*

Further tests with scatterplots showed similar results to those shown in **Figure 7**, with a close resemblance in the spectral signal between bare soil and impervious surface. Vegetation was clearly dissimilar to both the other classes. The largest dissimilarity between the classes was shown in the comparison between the Near Infrared band and the Red band.

The result from the land cover classification is shown in **Figure 8**. Grey symbolises areas classified as impervious surfaces, green illustrates vegetation and beige shows areas classified as bare soil. The bare soil areas in the exterior of the map were harvested fields and these takes up the majority of the bare soil coverage. These fields were also classified as impervious surfaces in some areas, due to the spectral similarities between the classes, as mentioned above. In the interior of the urban area, there were very few areas classified as bare soil.

Figure 8 *The result of the maximum likelihood classification. Impervious areas are shown in grey, bare soil is illustrated as beige and vegetation is shown as green.*

The distribution of the classes in the study area can be seen in **Table 8**. Vegetation dominated the study area with 66.9% coverage. Impervious surfaces were the second largest with 26.5% coverage and bare soil covered 6.6% of the area. As mentioned before, a majority of the bare soil coverage was beyond the populated area and consists of harvested fields.

Table 8 *The area distribution from the land cover classification. The areas are shown in hectares with the total coverage within the study area shown in percent.*

Category	Hectares	%
Impervious	1085.1	26.5
Bare Soil	269.7	6.6
Vegetation	2737.5	66.9

4.2.2 Accuracy assessment

Accuracy assessment of the land cover classification was performed using the error matrix approach, see **Table 9.** Columns represent the truth (reference data) and rows represent the mapped classification (based on the training sites). There was a total of 25 reference points in impervious surfaces, 4 for bare soil and 26 for vegetation. Of the total 4 points in bare soil, only 1 reference point was classified as bare soil. The other three points were situated on areas

classified as impervious surfaces. One point of impervious surface was classified as bare soil, resulting in a 50% error of commission for bare soil. The error of omission was 75%, with only one correctly classified point.

For impervious surfaces, the majority of the points were correctly classified, with a 20% error of omission. There were three points from bare soil classified as impervious surfaces, which lowered the errors of commission to 13%. There were 4 points from the reference data classified as vegetation instead of impervious surfaces and 1 point classified as bare soil.

Vegetation had a 0% errors of omission, meaning all the reference points were classified as vegetation in the map. 4 points of impervious surface were classified as vegetation, which gives and error of commission of 13.3%.

The overall accuracy of the classification was 85.45% (or a 14.55% overall error).

Table 9 *The error matrix for the result of the maximum likelihood classification. Columns depict the reference truth and rows represent the mapped result. Accuracy is shown as the error in percentage. The overall accuracy of the classification (OA) is shown in the bottom right corner of the table. The 95% confidence interval is 9.3%.*

Categories	**Impervious**	**Bare Soil**	**Vegetation**	**Total points**	**Error of Commission**
Impervious	20	3	0	23	13.04%
Bare Soil	1	1	0	2	50%
Vegetation	4	0	26	30	13.33%
Total points	25	4	26	55	
Error of Omission	20%	75%	0%		14.55%
95% confidence interval					5.5%-23.9% (9.3%)

The Kappa index of agreement for the different classes can be seen in **Table 10**. The Kappa index for both impervious and vegetation agreed with the accuracy and is at 0.76 and 0.75 respectively. The kappa index for bare soil was at 0.46, which also corresponds to the low accuracy in the error matrix. The overall kappa index for the classification was at 0.74 which can be considered fair to good (Fleiss 1981).

Table 10 *The Kappa index of agreement (KIA) for the three classes and the overall Kappa for the entire classification.*

Category	**KIA**
Impervious	0.76
Bare Soil	0.46
Vegetation	0.75
Overall Kappa	0.74

4.3.3 Inclusion of water as a class

Water was added to the classification from spectral characteristics gathered from the NIR band. The updated land cover classification is shown in **Figure 9**. The largest areas with water were located in the south western portion of the study area, which is where the water treatment facility of Lund is located. The areal distribution after identified water surfaces were added can be seen in **Table 11**.

The result shows that 4.45 ha of impervious surfaces have been reclassified into water. These areas were mostly in the inner urban environment in shadows from buildings, as seen in **Figure 9**. No areas with soil have been reclassified, while 19.6 ha of the vegetated areas have been changed into water. These areas were mostly in the south-western parts of the map.

Figure 9 *The maximum likelihood classification with water added to it. Impervious areas are shown in grey, bare soil is illustrated as beige and vegetation as green. Water is shown as light blue.*

Table 11 *The areal distribution of the land cover classification after water was added as a class. The areas are shown in hectares with the total coverage within the study area shown in percent.*

Classes	Hectares	%
Impervious	1080.6	26.4
Bare Soil	269.7	6.6
Vegetation	2717.9	66.4
Water	24	0.6

The misclassification of water within the populated areas of Lund is displayed in **Figure 10**. The map is centred on the main building in the hospital area in Lund. It is evident from the map that large areas close to buildings produce shadows in the Ortho-image. These shadows have a spectral signature that was misinterpreted as water due to the similarities with water in the NIR band. The map also displays the problems with similar spectral characteristics for impervious areas and bare soil (**Figure 8**), with certain parts of roofs being classified as bare soil.

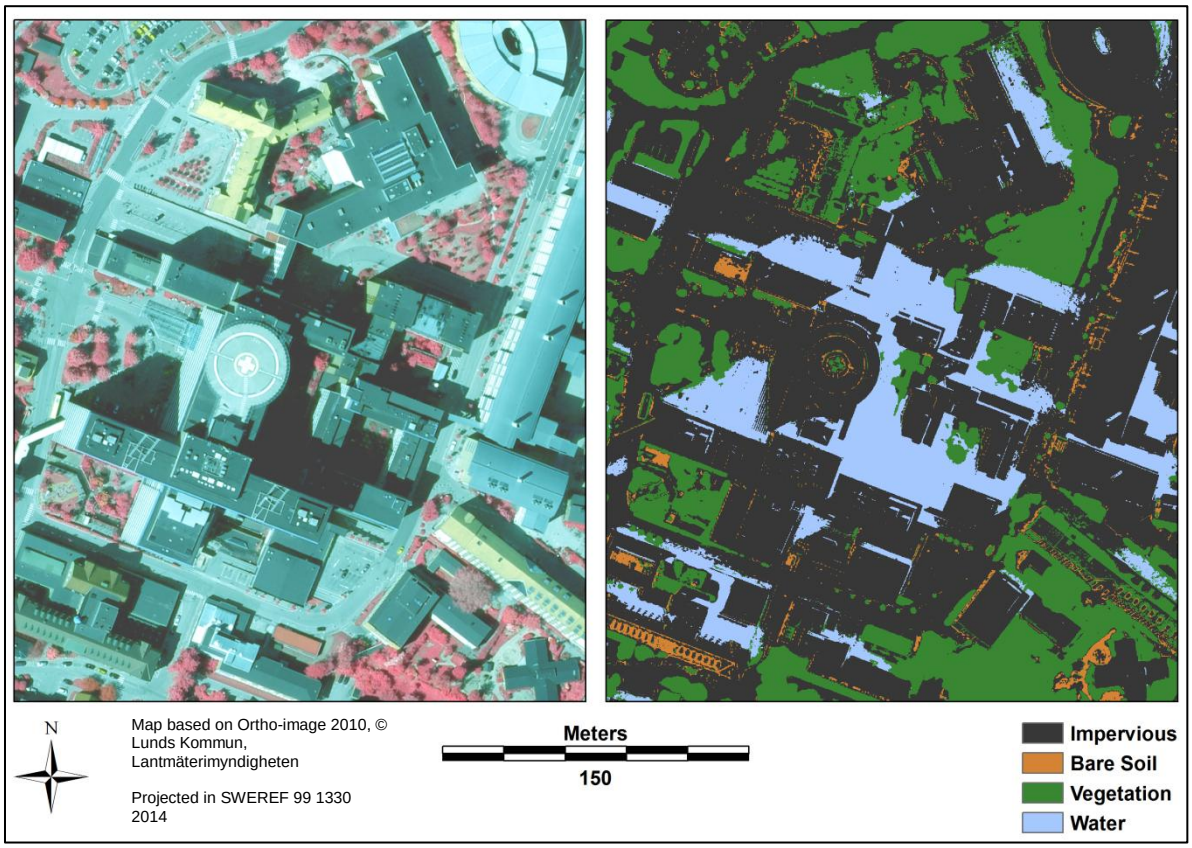

Figure 10 *Illustration of the misclassification of shadows as water in the land cover classification. Shadows from large buildings such as the hospital building in Lund are misinterpreted as water due to similarities in the spectral signature between water and shadows. The figure also illustrates impervious areas classified as bare soil, due to the spectral similarities between the two classes.*

4.3 Runoff model

The impervious surfaces (**Figure 9**) were selected and separated from the land cover classification, as seen in **Figure 11**. The buildings were removed from the impervious surface area since they were assumed pervious. The resolution of the map has been changed from the original 0.25 m to 2 m. The remaining areas were considered as pervious surfaces, and used the infiltration values presented in **Table 4.**

Figure 11 *The percentage impervious area within the study area. The range of imperviousness is shown as a proportion representing %. Buildings have been extracted from the impervious areas as these are assumed pervious.*

Figure 12 shows a zoomed in section from the map in **Figure 11**. This map displays the range of imperviousness presented in the result. As seen, the centre of an impervious area is classified as 100% impervious, while edges have a range from 0-100%. This is a result of the aggregation where the resolution is changed. The cells have been combined and the mean value of the impervious (μ) coverage has been calculated and applied to the new 2 metre cell.

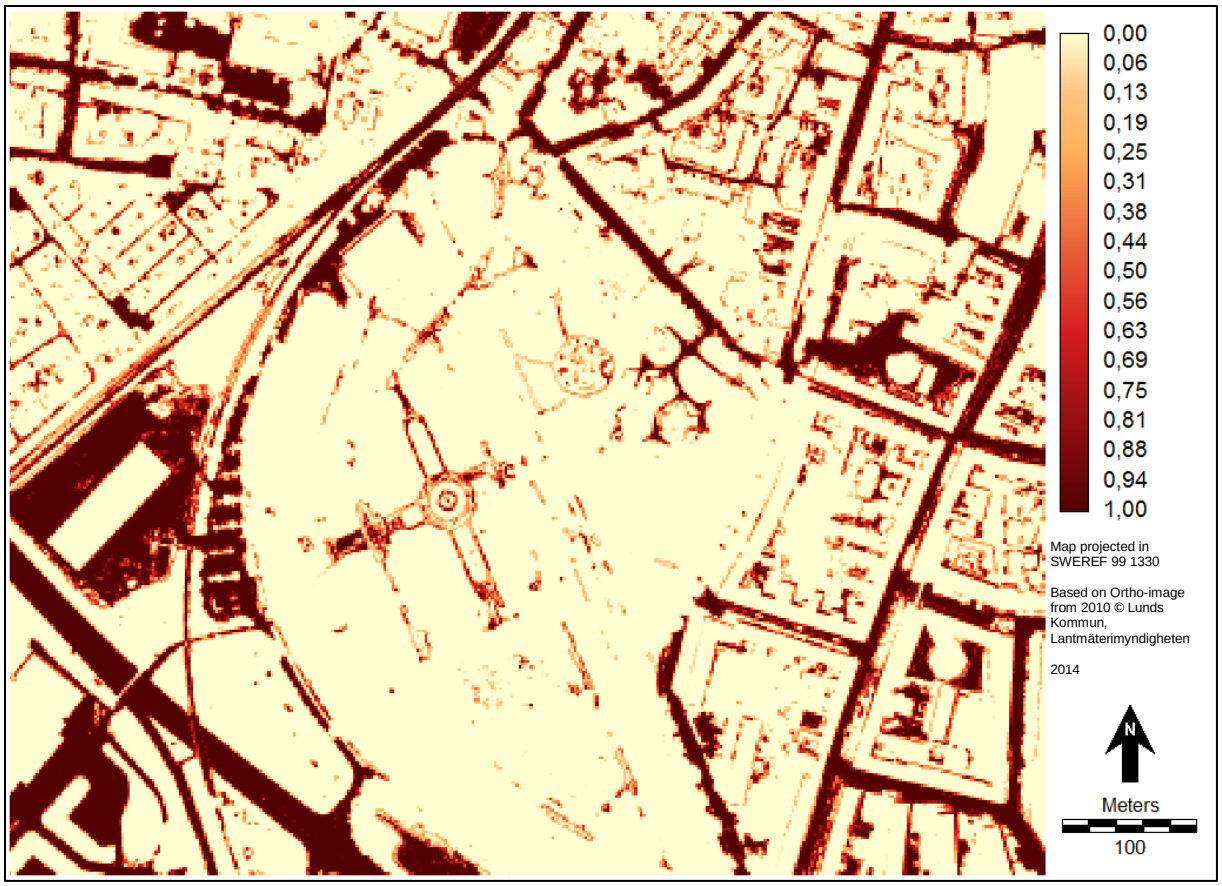

Figure 12 *The impervious surface area over a central part of Lund. The range of imperviousness is shown as a proportion representing %. Buildings have been extracted from the impervious areas as these are assumed pervious.*

After extraction of buildings from the classified impervious surfaces, the total area considered to be impervious was 786.4 ha, as seen in **Table 12**. This was a reduction of the impervious surface area of 294.2 hectares.

Table 12 *The areal distribution (in hectares) of impervious- pervious surface area within the study area after extracting buildings from the impervious surface class.*

Categories	Area
Impervious Surface	786.4 (ha)
Pervious Surface	3305.8 (ha)

4.4 Flow accumulation

The flow accumulation was based on the results from the runoff model, where cumulative infiltration was subtracted from the precipitation according to **Eq. 5**. The result (R), was used as a weight for the flow accumulation calculation. **Figure 13** illustrates the flow accumulation result over Lund Central station for the 3-hour, 1961-1990 scenario. In the map, areas with a volume equal to 0 (no accumulated flow) are not coloured, while areas with flow accumulation have a colour ranging from green (low) to red (high) depending on the volume

of accumulated runoff. As seen in the figure, the maximum volume accumulated flow for a cell within the study area is 607 m^3 of water for this scenario.

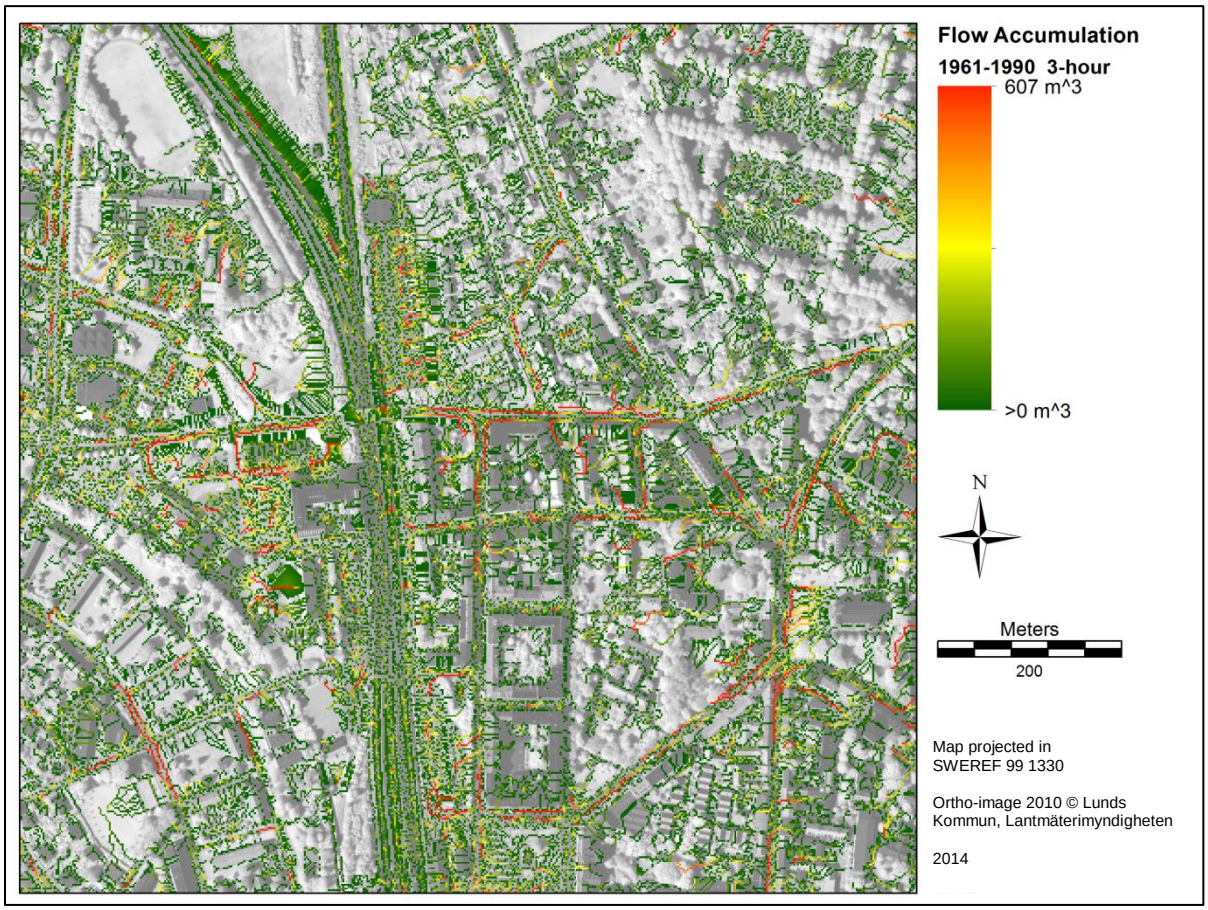

Figure 13 *Flow accumulation volume (m^3) in the central parts of Lund in the 3 hour scenario for 1961-1990. Red display high flow accumulation and green displays low volume. Cells with zero (0) accumulation are not displayed in the map. The area illustrated is the Lund Central station with surroundings.*

The result shows that pervious areas had almost no flow accumulation. High flow accumulation was located around impervious surfaces and especially roads.

4.5 Catchment delineation

The flow accumulation illustrates flow paths within the study area, but the main interest of this study was to locate and illustrate the upslope accumulation area. As describe in the method section (**Chapter 3.5.4**), catchments lying outside of the vicinity of the more densely populated area were removed. The secondary limitation was also applied, where each catchment must have a minimum 10 cell long flow path, where each cell has a runoff volume above the set threshold (90th-percentile).

Figure 14 displays the delineated catchments for the 3-hour scenario between 1961-1990. It illustrates catchments with high (198.8–415.5 m^3) accumulation of runoff in red, and areas with low (56.6–83.3 m^3) accumulated runoff in green. The catchments with the highest runoff

volume are located in road intersections or along road segments. Vegetated areas have very low representation in the result. Since buildings are considered to be of pervious nature in this study, areas with high a frequency of buildings are also to some extent underrepresented in the map. The largest accumulated runoff volume for this scenario is 415.5 m^3. The difference compared to the maximum volume presented in **Figure 14** is caused by the extraction of areas not included in the delineation process.

Figure 14 *Map displaying catchments with an accumulated runoff volume (m^3) over the 90-percentile for the 3-hour scenario between 1961-1990. Areas marked in red are areas with the highest runoff volume while green represents the lowest runoff volume.*

The numbers of catchments meeting the applied restrictions (the areas had to be in the vicinity of the urban area, not be composed exclusively of fields and the catchment had to be composed of 10 or more connected cells) for each one of the scenarios are presented in **Table 13**. The total number of catchments and the total contributing area (upslope accumulation area) are shown.

Table 13 *Numbers of catchment areas and the total contributing area (m^2) for the 6 different scenarios.*

Scenario	Number of catchments	Total contributing area (m^2)
3-hour 1961-1990	209	1,011,976
3-hour 1991-2012	226	1,062,632
24-hour 1961-1990	162	798,956
24-hour 1991-2012	162	804,144
72-hour 1961-2012	171	826,642
72-hour 1991-2012	1336	3,134,630

The result displays an increase of both catchments and contributing area with increased precipitation (**Table 5**). This relationship is especially seen for the 72-hour scenarios, where there is an 87% increase in number of catchments between the two setups.

Focus was put on the three catchments with the highest accumulated runoff volume for each of the six scenarios. These catchments are seen in **Figure 15**. The catchment areas are denoted as A, B and C as marked in the figure.

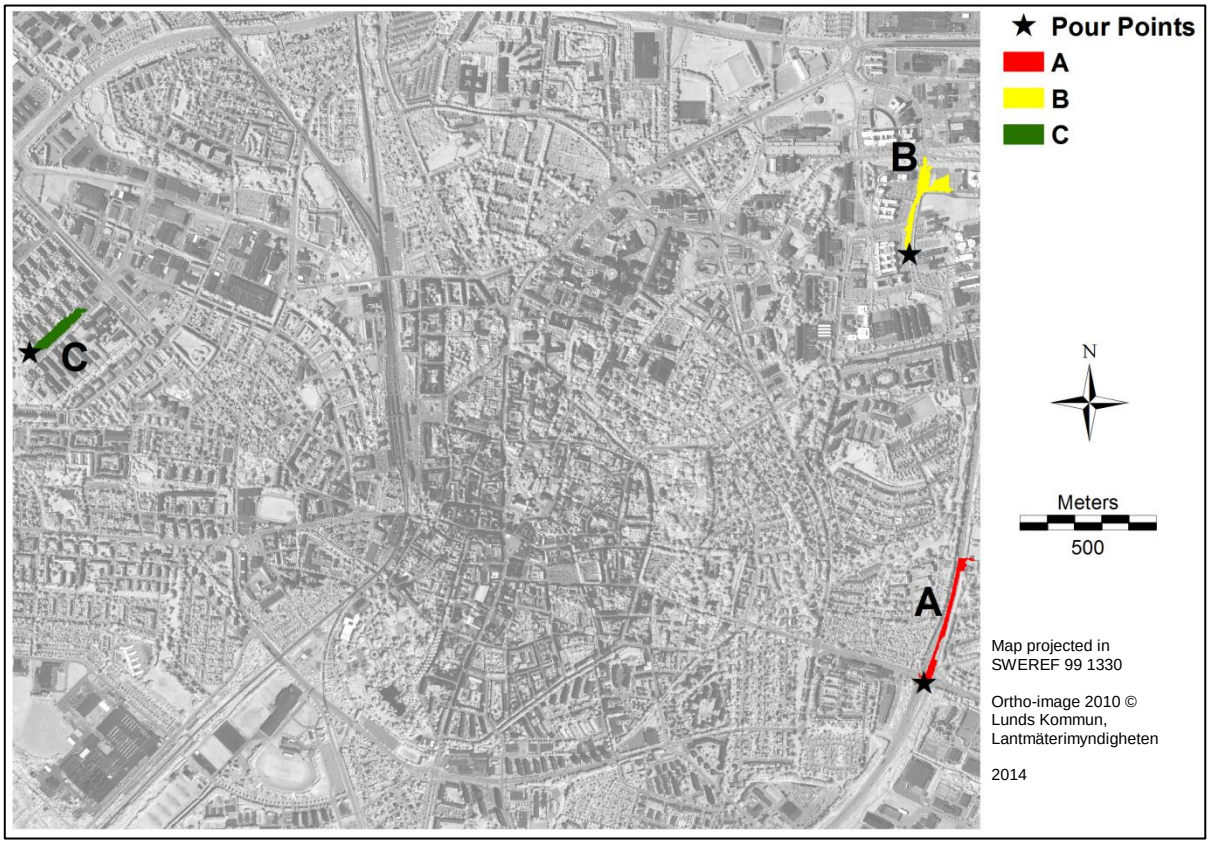

Figure 15 *The catchment areas with the highest runoff volume for all the 6 scenarios. Catchment A has the highest volume for all scenarios. Catchment B has the second highest runoff volume for both 3-hour scenarios and the 72-hour (1991-2012) scenario. Catchment C has the second highest volume for all 24-hour setups and in the 72-hour (1961-1990) scenario. Inlaid are the pour points for the three catchments.*

The catchments were situated at large connected impervious surfaces. Catchment area A is located along a motorway (E22) that goes through the south eastern parts of Lund. The area is situated close to an overpass of the highway. Area B is located in the area called Ideon, in the eastern parts of Lund. It consists of a road surrounded by gravelled parking lots. The last area, catchment C, is found in the south western parts of Lund, close to the urban outskirts. This area consists of a large parking lot, surrounded by a paved road.

In **Table 14**, the runoff volume for each catchment is presented, together with its runoff index. They are sorted alphabetically for each scenario. Catchment area A has the highest runoff volume for all scenarios, while the order for the second and third highest runoff volumes has changed.

Table 14 *The three catchments A, B and C with runoff volume (m^3) and runoff index (m^3/m^2) for the six different settings. Runoff index is the calculated runoff divided by the catchment area.*

Scenario	Catchment	Runoff (m^3)	Runoff index (m^3/m^2)
3-hour 1961-1990	A	415.5	0.04518
	B	402.1	0.03145
	C	363.4	0.04190
3-hour 1991-2012	A	430.3	0.04679
	B	419	0.03276
	C	376.5	0.04338
24-hour 1961-1990	A	390.3	0.04244
	B	335.5	0.02623
	C	342.6	0.03948
24-hour 1991-2012	A	404.4	0.04398
	B	348.3	0.02723
	C	354.7	0.04087
72-hour 1961-1990	A	434.6	0.04726
	B	366.8	0.02868
	C	393.4	0.04533
72-hour 1991-2012	A	1693.6	0.18424
	B	1512.4	0.11832
	C	1475.8	0.17004

The result shows that the difference in runoff between the scenarios corresponded closely to the difference in precipitation (**Table 5**). For the 3-hour and 24-hour scenarios there was a 3 % difference in precipitation between the two time periods (1961-1990 and 1991-2012). The runoff results show that for all selected catchments, this difference was carried over to the accumulated runoff. In the 72-hour scenario there was a ~30 % difference in precipitation between the two time periods, and the runoff showed a difference of almost 75 % for all three catchments.

Impervious surface coverage for each catchment (A-C) is shown as percent coverage in **Table 15**. The coverage can be compared to the overall statistics for all catchment areas in the 24-hour 1961-1990 scenario, seen in **Table 16**. Comparison shows that both areas A and C had a high percent impervious surface coverage (>81%), while catchment area B (58%) represented roughly the mean coverage (54%). Surface area for catchments A-C is also shown in **Table 15**, where area B is ~30% larger than both area A and C.

Table 15 *The impervious surface coverage for catchment areas A, B and C shown as percent coverage and the catchment's area shown in m^2.*

Catchment	Percent impervious coverage	Area (m^2)
A	81%	9196
B	58%	12789
C	83%	8678

Table 16 *Statistics for all 162 catchments in the 24-hour 1961-1990 scenario. Included are all catchments above the 90th-percentile threshold. "Maximum" represents the catchment with the highest impervious surface coverage, "Minimum" represents the catchment with the lowest impervious surface coverage and "Mean" represent the mean impervious surface coverage for all included catchment areas.*

Statistics for all catchments	Percent impervious coverage
Maximum	95%
Minimum	15%
Mean	54%

Based on the relationship between precipitation and runoff presented in **Table 14**, further analysis was focused on the time period 1961-1990.

Figure 16 illustrates the catchment areas with the highest runoff index for the remaining scenarios. The pour point (last receiving cell in the flow path) for each catchment is marked in the map by a star. By selecting catchments based on the runoff index, none of the previously described catchment areas (A-C) were amongst the top ones.

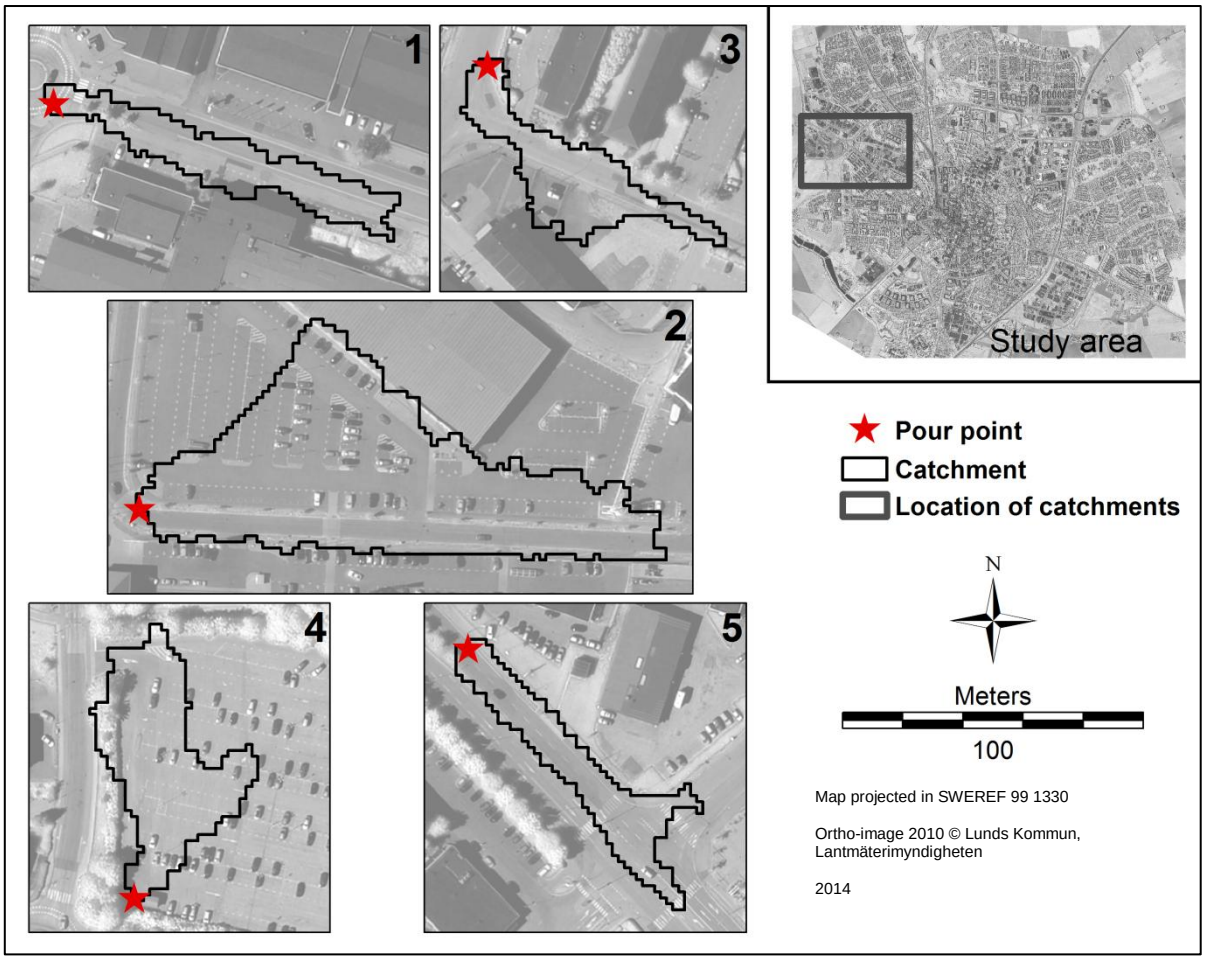

Figure 16 *Illustration of the catchments with the highest runoff index in the study area for all scenarios between 1961-1990. For the 3-hour scenario, catchments 1-3 respectively have the highest runoff index. For the 24 hour scenario, the order is 1, 4 and 3. In the 72 hour scenario the catchments with the highest runoff index are 1, 4 and 5 respectively. Inlaid is also the total study area with the location of the catchments. The pour point for each catchment is marked by a star.*

The catchments with the highest runoff index for the 3-hour scenario are marked 1-3 respectively. For the 24-hour scenario, the three catchments with the highest runoff index were number 1, 4 and 3 respectively and for the 72-hour scenario the order of the catchments were 1, 4 and 5.

In **Table 17**, each catchment's (1-5) runoff index is presented with the runoff volume and the flow path length. The flow path length was defined as the number of cells above the threshold volume for each scenario and above or equal to the restriction of at least 10 connected cells. When ordered by index value, area 4 was shown to have the 27th highest ranking in the 3-hour scenario. In the other two scenarios, it ranked on second place. All other catchment areas were among the top 6 when ordered by their index value. Flow path length was derived from the raster grid cells and indicates a distance of 2-2.8 meters. The flow path length altered with 1-4 cells between the different scenarios, with the highest increase seen in the 72-hour setting

for catchment 5. The runoff volumes were between 80%–65% lower for catchments 1-5 compared to catchments A-C, except for catchment 2 that had 19%–3% difference.

Table 17 *The three catchments with the highest runoff index for each scenario. The numbering of the catchment is based on Figure 15. "Order by Index" refers to ordering by runoff index value, with 1 being the catchment with the highest runoff index. For each catchment the runoff volume (m^3), runoff index and flow path length (number of connected cells above threshold value) is presented. The length in meter would alternate between 2 and 2.8 meter based on orientation of the flow within each cell.*

Scenario 1961-1990	Catchment (no.)	Order by index value	Runoff (m^3)	Runoff index (m^3/m^2)	Flow path length (cells)
3-hour	1	1	82.1	0.05225	23
	2	2	346.3	0.049979	63
	3	3	77.0	0.049745	10
	4	27	115.0	0.039499	13
	5	4	74.3	0.049005	15
24-hour	1	1	79.5	0.050562	23
	2	5	317.2	0.046483	63
	3	3	72.4	0.04678	10
	4	2	111.2	0.046997	13
	5	4	70.5	0.046485	16
72-hour	1	1	92.4	0.058752	25
	2	6	356.4	0.052231	63
	3	4	82.7	0.053393	10
	4	2	129.5	0.054736	14
	5	3	81.6	0.053845	19

The percent impervious surface coverage for catchment areas 1-5 is shown in **Table 18**. For all included catchments, the percent impervious surface coverage was above those for catchment areas A-C. Comparing the results for all catchments (**Table 16**), area 1 had the highest impervious surface coverage of all included catchment areas. Included in the table is also the surface area. Areas 1, 3 and 5 have similar area, while area 4 is ~34% larger in size. Area 2 is substantially larger (~77%) than areas 1, 3 and 5, and 65% larger than area 4.

Table 18 *The impervious surface coverage for catchments 1-5 shown as percent coverage and the catchment's area shown in m^2.*

Catchment	Percent impervious coverage	Area (m^2)
1	95%	1572
2	91%	6824
3	91%	1548
4	87%	2366
5	92%	1516

5. Discussion

5.1 Precipitation

The mean annual precipitation for Lund has increased over the last 50 years. This trend is supported in the results, as well as in Bengtsson and Rana (2014). The main reason for this increase is thought to be a change in the winter and autumn precipitation, while summer precipitation has been stable (Bengtsson and Rana 2014). There are reports suggesting a decrease in summer precipitation for the southern parts of Sweden (Dahlström 2006), but Bengtsson and Rana (2014) argue that this decrease is only seen in observations for the month of August. The decision to focus on summer precipitation in this study is based on the fact that the most extreme storm events occur during the summer months (**Table 5**). There are events during other seasons that comes close to the intensity seen in summer precipitation, but most extreme events occur during summer (Bengtsson and Rana 2014).

For the closely located city of Malmö, a study by Bengtsson and Milloti (2010) shows that about 50% of the extreme events from 1980 until 2007 had a duration of less than 5 h. The highest precipitation amounts came over a time period of at least 9 h. The relatively closeness (~16 km from centre to centre) between the two cities would suggest that a similar result would be expected in Lund. These results suggest the need to examine the response to extreme storm events over different durations, as done in this study.

There are small differences in this study's results when compared to the study by Bengtsson and Rana (2014). In their report, the same region is analysed but over a longer time period (1873-2011). Bengtsson and Rana (2014) state that many of the largest rainfall events occurred in the 1940s and that there is a reduction in magnitude of the 50-year and 100-year rain events for the later part of the 20th century. Since 1980, 50-year storms have decreased from about 78 mm/day to 65 mm/day in 2011. They also state that the most extreme events (>40 mm/day) seem to be random and not to be strongly correlated to annual precipitation, nor to frequency of moderate rains. The result from this study indicates that there might be a slight increase in frequency of extreme events during the last 20 years (1991-2012). For the first 30 years (1961-1990), only 5 extreme events were recorded, while a total of 6 events were recorded for the last 20 years. While there might be an increase in frequency, the magnitude does not seem to have increased.

In this study the assumption was made that precipitation was homogenous over the study area. This simplification stems from the low resolution of the precipitation data, where one

measurement had to represent the whole area. A higher resolution of the precipitation data is not available without interpolation or radar analysis, and was not a focus of the study. The actual volumes from flow were not the main goal of the analysis, but rather the possibilities and locations of surface flows.

The inclusion of future precipitation presented in this study was aimed at predicting future extreme events. Due to the low temporal resolution of the data, it is hard to predict any specific trend or result. The scenario used (RCP 8.5) is attuned to continued high levels of CO_2 emissions. The model indicates an increase in precipitation, but the spread is large for the prediction. The decision to use the more extreme RCP scenario was to try to portray a large difference compared to the control time period of 1961-1990. The aim of this study was not focused on evaluating the effects from different scenario data, but to use a scenario that produced large volumes of precipitation to test the model.

5.2 Impervious surface analysis

The accuracy of land cover classifications can be hard to evaluate. To ensure that the model was sufficiently accurate to be used as input for the runoff model, the result was compared to classifications performed using a secondary approach where samples not collected in the field were used (see **Chapter 3.5.1**). The assessment of this result suggested a better fit for the secondary approach, but visual inspection and comparison deemed the field sampled classification as a more accurate representation of the impervious surfaces within Lund. Using definitions proposed by Fleiss (1981), an overall Kappa of 0.74 can be described as a fair to good result which was considered a feasible result.

The accuracy of a land cover classification relies heavily on the gathered field samples. A sufficient number of samples are needed to accurately classify each land cover class. As mentioned in **Chapter 2.3**, 50 samples from each class could be needed to classify an image accurately (25 as training sites and 25 as reference) (Congalton and Green 1999). Bare soil was represented by only 7 samples, with 3 used for the classification and 4 as reference points. Based on the statement by Congalton and Green (1999), this would not be considered a sufficient amount of samples to correctly classify the category in the land cover classification. The result (**Table 9**) also indicated that the accuracy of the classification was questionable at best. A different approach could have been to neglect sampling this land cover type entirely (Han and Burian 2009), considering that it did not account to a substantial part of the urban texture. This would adversely affect the classification of areas outside the

urban limit, which could inadvertently be misclassified as impervious surface. This would increase the impervious surface coverage and include larger areas as urban then was the case in the results given in this study. A way to circumvent this could have been to create an urban mask, using e.g. supervised or unsupervised classifications (Dams et al. 2013). This approach was, however, not performed, since it would be based on visual interpretation of the Ortho-image, which would assume that both the interpretation and the classification are correct. Errors produced this way would be blamed on the classification, thus lowering the classification accuracy (Congalton 1991).

The number of categories used in the land cover classification could also affect the accuracy of the result. As mentioned in **Chapter 3.5.1**, water was excluded from the maximum likelihood classification. This was done based on spectral similarities between water and shadows in the Ortho-image. Naturally, shadows are not a valid land cover class and should not be sampled as such. Hypothetically, shadows could appear in the same spot and size if collected at the same time of day, and on the same Julian day as the Ortho-image. While this might hypothetically be true, during field sampling this is not guaranteed. Consequently, it was decided that water would be added to the classification based on information gathered from only the near infrared band. This did not prevent shadows from being classified as water, but reduced the quantity of misclassified areas. This method added an undetermined level of uncertainty to the land cover classification, since water was not included in the accuracy assessment result. The quantity of changed impervious surface pixels was relatively low (0.01 percentage points, see **Table 8** and **Table 11**) and was not considered large enough to change the end result significantly.

High resolution imagery was chosen over lower resolution imagery to decrease the influence of mixed pixels (Lu et al. 2011). This decision introduced other factors causing spectral confusion, such as the afore mentioned shadows. Shadows were present in large parts of the inner urban areas. When not included as a class in the maximum land cover classification, they caused confusion and spread within all classes. Shadows produced by buildings and shadows produced by trees are spectrally very similar. The result of this confusion can be seen in the accuracy assessment (**Chapter 4.2.2**), where samples of impervious surfaces have been classified as vegetation. Naturally, shadows alone were not the sole reason for misclassification and spectral confusion. Bare soil and impervious surfaces can be spectrally very similar (Lu and Weng 2004), as seen in **Figure 7.** In certain areas, roofs with high reflectance were classified as bare soil (**Figure 10**). This misclassification could perhaps have

been avoided by sampling impervious surfaces as several classes, as done by Han and Burian (2009). Although this approach could prove to produce a more accurate result, the sampling would prove very difficult and time consuming. The use of a high resolution image also increases the "salt and pepper" effect in the classification process (Lu et al. 2011). The "salt and pepper" effect is when small clusters or separate pixels are classified differently than surrounding pixels. This effect is reduced by the aggregation done in the study and was not considered to influence the input to the runoff model.

The argument to increase the number of sub-classes could be applied to the all categories. An increased number of sub-classes for the pervious surfaces could have proven to increase overall accuracy. But, as seen in **Figure 7**, vegetation is already spectrally dissimilar compared to impervious surfaces, and bare soil had minimal coverage throughout the study area. Therefore, an increase of sub-classes in this category was not perused.

To summarise the discussion of the impervious surface analysis, misclassification in the land cover analysis is thought to be mainly attributed to the confusion caused by shadows and spectral similarities between impervious surfaces and bare soil. The lack of field samples of bare soil could also influence the accuracy greatly. The result (**Table 9**) indicates a very low accuracy on predicting areas covered with bare soil.

5.3 The runoff model

The runoff model used in this study is based on the model created by Chen et al. (2009), with the exclusion of storm water drainage. It includes precipitation, infiltration and impervious surfaces. Precipitation was implemented in the model as a homogenous layer with equal volumes for each cell in each scenario. This was a large simplification of the natural phenomenon that is precipitation. Wilson et al. (1979) showed that spatial distribution and precipitation accuracy have a marked influence on runoff volumes in small catchments. To evaluate the influence of the static representation used in this study, tests could have been performed with spatially distributed precipitation events. However, the main purpose of the model was not to correctly represent runoff for an occurred event, but rather to locate areas of interest when high volumes of precipitation occur. The implementation of homogenous precipitation functions more as a design storm event than an actual storm. Theoretically, large precipitation volumes are possible for each cell in the study area. Therefore, the use of a spatially non-distributed precipitation pattern was considered a valid approach in this study.

Infiltration was applied to the model on areas with no impervious surface, in accordance with **Equation 3** and **4**. Because of the aggregation of the impervious surface layer to match the DEM, cells could have a fraction of infiltration based on the impervious coverage. Infiltration was applied as a subtraction of the received precipitation for each cell, with the remaining volume set as runoff. The infiltration capacity was derived from an investigation of the dominant soil type in the study area. This assumes that all areas with infiltration have the same capacity, when in fact the urban environment consists of several sources of infiltration (Mohrlok et al. 2008). Proper implementation of infiltration would include e.g. slope and prior wetness in soil. Prior wetness would e.g. affect ponding times (the time when infiltration capacity is reached) and would change infiltration rates (Diskin and Nazimov 1996). Areas are also under constant change in an urban environment and to locate and quantify the impact of each parameter is a difficult task (Mohrlok et al. 2008). Infiltration was therefore implemented mainly to separate areas of impervious nature from permeable surfaces. Since the dominant soil type according to SGU (2014) is clay based material, the properties of clay was chosen to represent infiltration rates.

The last parameter in the runoff model was the impervious surfaces. It was based on the aggregated result from the impervious surface analysis. The accuracy of this result has been discussed in the previous chapter. In contrast with infiltration, precipitation over cells composed of impervious surfaces was assumed to become runoff. Areas with both impervious surface and pervious surface had runoff based on the fraction of imperviousness. The implementation relied only on the result from the impervious surface analysis. The exclusion of buildings as a source of impervious surface was made based on lack of information regarding practice and quantity of roof drainage. A contributing factor was also that the DEM was levelled at location of buildings, which influenced the implementation of the runoff model in the GIS environment.

Another large unknown factor in the model is the lack of information regarding storm water drains. Drains would normally be included in a runoff model to account for anthropologically removed water in an urban environment (Chen et al. 2009), but were not included in the study on the grounds of a lack of information regarding their location and limited time to properly implement the equations in the GIS environment. The lack of this information naturally affects the outcome of the model, overestimating runoff volumes in certain areas. Areas that are normally controlled by extensive drainage could be included as areas with high runoff

volume. The insufficient information renders the result biased towards large connected impervious surfaces.

5.4 The digital elevation model and flow direction

Since a DEM is the main input to a hydrological analysis (Zhou et al. 2011), the quality of the DEM is of great importance. An obvious source of error in any analysis performed with a DEM, is the assumptions introduced by its structure (Zhou and Liu 2004). The regular sampling scheme used in a gridded DEM can produce "octant bias", presented by obvious visual and numerical error patterns (Zhou and Liu 2004). This means that the structure and the resolution of the DEM might introduce errors based on missing information or assumed patterns caused by a regular structure. The quality of the DEM used in the study was not investigated, but was assumed to be sufficient based on its source and characteristics. The high resolution portrays an accurate representation of the terrain in the study area. However, the pre-processing done by BLOM Sweden AB prior to acquiring the DEM, proved to alter the expected result of the flow accumulation. As mentioned in the previous chapter, areas with buildings had been flattened to the level of the surroundings, which made it possible for flow to pass through built up areas unhindered. If this attribute of the DEM had been discovered earlier in the analysis, the DEM could perhaps have been changed or altered to better suit the analysis. One way to do that would have been to use the vector layer containing buildings to raise the DEM significantly (e.g. 100m) at those locations. This would have prevented the model from directing flow over areas with buildings and directed flow along other paths.

The choice of algorithm to use when conducting an analysis, such as flow direction, can be influenced by the quality of the DEM. In this study, a SFD (D8) was used to produce the flow directions. There are arguments that the use of such an algorithm introduce errors based on the limitations of the algorithm (Zhou and Liu 2004; Seibert and McGlynn 2007; Zhou et al. 2011). A different approach would have been to use another type of flow direction algorithm, such as a multiple flow direction (MFD) algorithm. This option was however limited based on the decision to use built in functions in ArcGIS.

5.5 Accumulated flow and catchment delineation

Accumulated flow volumes were calculated from the flow direction in combination with the runoff model result. It derives flow paths with surface water runoff volumes for each separate route within the study area. The paths with the highest runoff volumes were then used to calculate the upslope catchment area. The catchment area calculations were based on the flow direction result (Jenson and Domingue 1988) and its accuracy was dependent on the accuracy of the flow direction model and the DEM.

The implementation of the runoff model in a GIS environment proved to result in a number of difficulties. The runoff model was applied to the flow accumulation calculations in a multiplicative manner. It was not realised in an early stage how this would affect the prediction of runoff volumes. The applied runoff model consisted of a raster with constant values for each cell, representing the runoff. This runoff was then to be routed by the flow direction to its end destination. However, since infiltration was applied to the runoff, infiltrating cells produced non to low volumes of runoff. With a multiplicative implementation, these cells effectively acted as infinite sinks. Small errors produced by the impervious surface analysis then became problems when otherwise uninterrupted impervious surfaces were cut off by e.g. shadows, misclassified as pervious surfaces. This effect could have resulted in misplaced pour points which results in wrongfully selected catchments.

The model also lacked a temporal component, which also affect the implementation of infiltration. The built in flow accumulation function in ArcGIS does not provide functionality for iterations. This means that it was not possible to check for previous conditions. Chen et al. (2009) describe in their report how a model could check for previous conditions and allow for flow routing over infiltrating cells if the infiltration capacity is reached. Their implementation is however based on stand-alone programming and does not use the built in tools to acquire the result.

To try to circumvent the described problems, an alternative approach was tested where flow accumulation was calculated solely based on the flow direction. The runoff was then calculated by multiplying the flow accumulation result with the homogenous precipitation layer. This resulted in a theoretical model where all precipitation became runoff. Infiltration was then applied using subtraction. This approach produced a much different result than expected, since the infiltration was applied after the accumulated flow had reached its pour point. Most areas with high runoff volumes were located outside the urban area. Catchment

areas outside the city limit proved to be much bigger and have longer flow paths, resulting in very high runoff volumes. When extracting catchments based on the 90th-percentile runoff volume, no areas within the city were included. This result rendered the approach not suited for the aim of finding areas within the urban environment. An alteration of this approach could have been used, by manually selecting pour points from the flow accumulation to use in the catchment delineation. However, this is a very time consuming approach and would effectively rely on the user to find all flow paths of interest for each scenario.

Even with the described problems and a probable bias towards impervious surfaces in general, the resulting catchments (A-C, **Figure 14**) are considered interesting. They consist of large connected impervious areas with a potential to create large volumes of surface runoff as seen in the result (**Table 14**). Even with a bias, impervious surfaces are at an increased risk of flooding, or contributing to flooding, with higher frequency and larger runoff volumes compared to pervious surfaces (Thurston et al. 2003; Veracka 2013). Since the study does not include information regarding storm water drains, it is hard to predict if the selected catchment actually flood in the event of a storm. The result should be used more as a "worst case scenario" material, with the portrayed catchments being the most likely candidates to flood or to contribute to flooding nearby.

Other factors not included in the calculations were flow velocity and surface roughness. Different surface properties affect flow velocities in different ways (Henderson and Wooding 1964). Flow velocity would affect the response time in pour points and for large areas. The time it would take for water to reach the pour point is naturally longer. A slow response time would put lower pressure on potentially present storm water drains, and enable them to drain efficiently. In an attempt to account for response times, the runoff index was calculated. It is composed of runoff volume and the area of the catchment, and is essentially the height of the water level if the accumulated runoff volume was evenly spread throughout the catchment. The theory behind the index was that large areas would have longer response times. By dividing runoff volume with the contributing area, larger areas would have lower index values. A low index value was thought to indicate on slow response time, meaning that the most interesting areas were those with high index values, or comparably high water level. A side effect of this was a bias towards small areas. In an attempt to compensate for this, a limitation was introduced by only including areas with flow path lengths above 10 cells (20-28 meters). This limitation was derived solely based on visual interpretation of the results. Many small catchments consisted of input from only a single cell which was considered too

small to be included in further analysis. When ranked by runoff index, none of the previous catchments (A-C) were among the top 3. These new smaller areas (1-5, **Figure 15**) were thought to have faster response times from rainfall to potential flooding. Although not producing equally high volumes of precipitation when compared to the top catchments ranked by runoff (A-C), these areas are thought to produce considerable volumes with faster response times. The risk of flooding in these catchments was thought to be higher than for those ranked only by runoff volume. With faster response times, more pressure is added to any existing storm water drains. The new areas (1-5) are thought to have the highest flood potential in urban Lund.

Bengtsson (2009) writes in his report that Lund has a generally low risk of flooding caused by rain compared to other cities. The topography of Lund makes it so that most of the city's storm water drains lies in a slope towards the receiving waters. Most of the floods that have occurred within the urban limit are caused by decreased potential of existing drains. The biggest problems is often caused by prolonged rains where large volumes of water from saturated pervious surfaces contribute to flows from the impervious surfaces and together exceed the capacity of the storm water drains.

6. Conclusions

The decision to use measured precipitation data as input for the runoff model was based on the belief that precipitation would have increased in the study area during the studied time period. It was expected that there would be an increase in both magnitude and frequency of extreme events (>40 mm/day), especially during the summer season. From the result it can be concluded that there has been an increase in yearly precipitation (1.7%) over the time period, but the increase in magnitude of extreme events is not seen. With the expected increase, there would have been a larger difference in runoff volumes for the studied catchment areas. The result from the runoff model could have been reached without the inclusion of measured data, which would have saved both time and effort in locating areas of interest. As seen from the result, there are only small differences between the different time periods (1961-1990 and 1991-2012) concerning which areas are most prone to flooding. Simulation of extreme events would have produced the same or similar results.

The runoff model used in this study needed an accurate representation of the impervious surfaces within the study area to produce adequate results. This was achieved using high resolution Ortho-imagery to produce a land cover classification. From the results in this study, it can be stated that impervious surfaces are of great importance when conducting a runoff analysis in an urban environment. The result from the implementation of the runoff model in a GIS environment together with flow accumulation showed that most areas with high flow accumulation (above a 90th-percentile threshold) consisted of mainly impervious surfaces with a 54% mean coverage for these areas. However, it can be argued that even though the results indicate that impervious surfaces are the main source of flow accumulation, the implementation of factors influencing the flow accumulation (e.g. infiltration) is of importance. Therefore, it cannot be concluded whether impervious surfaces are the most important factor to consider. To answer this question, the study would need to include more parameters that influence the runoff and a use a different approach of implementing infiltration. The results from this study produce a large bias towards impervious surface due to an overestimation of infiltration in pervious areas. It is also worth mentioning that the results from using high resolution imagery (0.25 meters) could likely have been achieved with a lower resolution. Even though the high resolution decreased the mixed pixel problem, it introduced other problems related to the classification of shadowed areas and water.

The results of the combined runoff and flow accumulation model produced catchments with similar surface coverage. It can be concluded that the main surface coverage for the areas with

the highest flow accumulation was impervious surfaces, with >58% coverage. The location of these areas is seen in **Figure 15**. A more detailed representation of the surface coverage could perhaps have been achieved by using sub-classes for the two categories (impervious and pervious). It is possible, due to the simplified approach of using one class to represent impervious surfaces, that catchments could have had a different impervious surface coverage than presented in the study, and that the land cover classification overestimated the impervious surface coverage.

The areas with the highest potential runoff accumulation are not necessarily those areas that are most prone to flooding. It can be concluded that those areas have the potential to accumulate large volumes of runoff in the event of extreme precipitation (see **Table 14**), but they are all fairly large (0.87 ha to 1.28 ha). As discussed in **Chapter 5.5**, larger areas could have longer response times from rain to potential flooding. To compensate for this, the study made use of a runoff index (water level height). It is suggested that results based on this index portrays a more accurate representation of areas most prone to flooding.

7. References

Achberger, C., M. L. Linderson, and D. Chen. 2003. Performance of the Rossby Centre regional atmospheric model in Southern Sweden: comparison of simulated and observed precipitation. *Theoretical and Applied Climatology,* 76**:** 219-234. DOI: 10.1007/s00704-003-0015-6

Barbosa, A. E., J. N. Fernandes, and L. M. David. 2012. Key issues for sustainable urban stormwater management. *Water Research,* 46**:** 6787-6798. DOI: http://dx.doi.org/10.1016/j.watres.2012.05.029

Bengtsson, L. 2009. Översvämning i stadens vattensystem. In *Forskning & Framtids forskningsprojekt*. http://www.lansforsakringar.se/globalassets/aa-global/dokument/ovrigt/aa-om-oss/forskning/00000-oversvamning-i-stadens-vattensystem.pdf: Länsförsäkringar.

Bengtsson, L., and S. Milloti. 2010. Extreme storms in Malmö, Sweden. *Hydrological Processes,* 24**:** 3462-3475. DOI: 10.1002/hyp.7768

Bengtsson, L., and A. Rana. 2014. Long-term change of daily and multi-daily precipitation in southern Sweden. *Hydrological Processes,* 28**:** 2897-2911. DOI: 10.1002/hyp.9774

Bhend, J., and H. von Storch. 2008. Consistency of observed winter precipitation trends in northern Europe with regional climate change projections. *Climate Dynamics,* 31**:** 17-28. DOI: 10.1007/s00382-007-0335-9

Burns, M. J., T. D. Fletcher, C. J. Walsh, A. R. Ladson, and B. E. Hatt. 2012. Hydrologic shortcomings of conventional urban stormwater management and opportunities for reform. *Landscape and Urban Planning,* 105**:** 230-240. DOI: http://dx.doi.org/10.1016/j.landurbplan.2011.12.012

Chen, J., A. A. Hill, and L. D. Urbano. 2009. A GIS-based model for urban flood inundation. *Journal of Hydrology,* 373**:** 184-192. DOI: http://dx.doi.org/10.1016/j.jhydrol.2009.04.021

Congalton, R. G. 1991. A review of assessing the accuracy of classifications of remotely sensed data. *Remote Sensing of Environment,* 37**:** 35-46. DOI: http://dx.doi.org/10.1016/0034-4257(91)90048-B

Congalton, R. G., and K. Green. 1999. *Assessing the Accuracy of Remotely Sensed Data: Principles and Practices*. Lewis Publishers, Boca Raton, FL.

Dahlström, B. 2006. Regnintensitet i Sverige - en klimatologisk analys (Storm intensities in Sweden - a climatological analysis). *VA-Forsk rapport NR 2006-26, 69 s.*

Dams, J., J. Dujardin, R. Reggers, I. Bashir, F. Canters, and O. Batelaan. 2013. Mapping impervious surface change from remote sensing for hydrological modeling. *Journal of Hydrology,* 485**:** 84-95. DOI: http://dx.doi.org/10.1016/j.jhydrol.2012.09.045

Diskin, M. H., and N. Nazimov. 1996. Ponding time and infiltration capacity variation during steady rainfall. *Journal of Hydrology,* 178**:** 369-380. DOI: http://dx.doi.org/10.1016/0022-1694(95)02798-X

ESRI. 2014. Sverige Kommungränser (Municipality Borders Sweden). Retrieved 2014-08-11, from. http://www.arcgis.com/home/item.html?id=41f5d23fef8f410590f2d934c7dba81a

Fleiss, J. L. 1981. *Statistical methods for rates and proportions (2nd ed.)*. John Wiley, New York.

Floriani, L., and P. Magillo. 2009. Digital Elevation Models. In *Encyclopedia of Database Systems*, eds. L. Liu, and M. T. ÖZsu, 817-821 pp.: Springer US.

Foody, G. M. 2002. Status of land cover classification accuracy assessment. *Remote Sensing of Environment,* 80**:** 185-201. DOI: http://dx.doi.org/10.1016/S0034-4257(01)00295-4

Giorgi, F., and P. Lionello. 2008. Climate change projections for the Mediterranean region. *Global and Planetary Change,* 63**:** 90-104. DOI: http://dx.doi.org/10.1016/j.gloplacha.2007.09.005

Green, W. H., and G. A. Ampt. 1911. Studies on soil physics. Part I: the flow of air and water through soils. *Journal of Agriculture Science,* 4 (1)**:** 1-24.

Han, W. S., and S. J. Burian. 2009. Determining effective impervious area for urban hydrologic modeling. *Journal of Hydrologic Engineering,* 14**:** 111-120. DOI: 10.1061/(ASCE)1084-0699(2009)14:2(111)

Henderson, F., and R. Wooding. 1964. Overland flow and groundwater flow from a steady rainfall of finite duration. *Journal of Geophysical Research,* 69**:** 1531-1540.

Holmgren, P. 1994. Multiple flow direction algorithms for runoff modelling in grid based elevation models: An empirical evaluation. *Hydrological Processes,* 8**:** 327-334. DOI: 10.1002/hyp.3360080405

Hornberger, G. M. 1998. *Elements of Physical Hydrology*. Johns Hopkins University Press.

Jenson, S., and J. Domingue. 1988. Extracting topographic structure from digital elevation data for geographic information system analysis. *Photogrammetric engineering and remote sensing,* 54**:** 1593-1600.

Kjellström, E., Hansson, U., Jones, C., Nikulin, G., Strandberg, G., Ullerstig, A. 2009. Changes in the wintertime temperature climate as deduced from an ensemble of regional climate change simulations for Europe. In *Rossby Centre Newsletter,* 9-15. http://www.smhi.se/polopoly_fs/1.2923!/RCnews_may_2009.pdf.

Kottek, M., J. Grieser, C. Beck, B. Rudolf, and F. Rubel. 2006. World Map of the Köppen-Geiger climate classification updated. *Meteorologische Zeitschrift,* 15**:** 259-263. DOI: 10.1127/0941-2948/2006/0130

Lantmäteriet. 2014. Ladda hem gratis Sverigekartor (Download free Sweden maps). Retrieved 2014-08-11 2014, from. http://www.lantmateriet.se/sv/Kartor-och-geografisk-information/Kartor/Sverigekartor/Ladda-hem-/#faq:Sverige-11-miljoner

Li, M., X. Hou, M. Zhu, and C. Shen. 2010. Extraction and application of impervious surface area in Yellow River Delta. In *Geoscience and Remote Sensing (IITA-GRS), 2010 Second IITA International Conference*, 634-637. Qingdao: IEEE.

Lillesand, T. M., R. W. Kiefer, and J. W. Chipman. 2008. *Remote sensing and image interpretation*. John Wiley & Sons.

Linderson, M.-L. 2002. The Spatial Distribution of Precipitation in Scania, Southern Sweden. Observations, model simulations and statistical downscaling. PhD Thesis Lund University

Lu, D., S. Hetrick, and E. Moran. 2011. Impervious surface mapping with QuickBird imagery. *International journal of remote sensing,* 32**:** 2519-2533.

Lu, D., and Q. Weng. 2004. Spectral mixture analysis of the urban landscape in Indianapolis with Landsat ETM+ imagery. *Photogrammetric Engineering & Remote Sensing,* 70**:** 1053-1062.

McCoy, R. M. 2005. *Field Methods in Remote Sensing*. Guilford Press.

Meyer, S., T. Salem, and J. Labadie. 1993. Geographic Information Systems in Urban Storm-Water Management. *Journal of Water Resources Planning and Management,* 119**:** 206-228. DOI: doi:10.1061/(ASCE)0733-9496(1993)119:2(206)

Mohrlok, U., L. Wolf, and J. Klinger. 2008. Quantification of infiltration processes in urban areas by accounting for spatial parameter variability. *Journal of Soils and Sediments,* 8**:** 34-42. DOI: 10.1065/jss2007.05.225

Morgan, R. P. C. 2005. *Soil Erosion and Conservation*. Blackwell Publishing.

MSB. 2011. Översvämningsdirektivet (The Flooding Directive). Retrieved 2014-07-30, from. https://www.msb.se/oversvamningsdirektivet

O'Callaghan, J. F., and D. M. Mark. 1984. The extraction of drainage networks from digital elevation data. *Computer Vision, Graphics, and Image Processing,* 28**:** 323-344. DOI: http://dx.doi.org/10.1016/S0734-189X(84)80011-0

Pilesjö, P., Q. Zhou, and L. Harrie. 1998. Estimating Flow Distribution over Digital Elevation Models Using a Form-Based Algorithm. *Geographic Information Sciences,* 4**:** 44-51. DOI: 10.1080/10824009809480502

Riahi, K., S. Rao, V. Krey, C. Cho, V. Chirkov, G. Fischer, G. Kindermann, N. Nakicenovic, et al. 2011. RCP 8.5—A scenario of comparatively high greenhouse gas emissions. *Climatic Change,* 109**:** 33-57. DOI: 10.1007/s10584-011-0149-y

Richards, J. A. 1986. *Remote Sensing Digital Image Analysis: An Introduction.*: Berlin, Springer.

Richards, J. A., and X. Jia. 2006. *Remote Sensing Digital Image Analysis*. Springer Berlin Heidelberg.

SCB. 2014. Statistisk årsbok 2014 (Statistical Yearbook 2014). 618 s. Statistiska centralbyrån (Statistics Sweden).

Seibert, J., and B. L. McGlynn. 2007. A new triangular multiple flow direction algorithm for computing upslope areas from gridded digital elevation models. *Water Resources Research,* 43**:** W04501. DOI: 10.1029/2006WR005128

SGU. 2014. Kartgenerator (Map generator). Retrieved 2014-04-11, from. http://maps2.sgu.se/kartgenerator/maporder_sv.html

Thomas, N., C. Hendrix, and R. G. Congalton. 2003. A comparison of urban mapping methods using high-resolution digital imagery. *Photogrammetric engineering and remote sensing,* 69**:** 963-972.

Thurston, H., H. Goddard, D. Szlag, and B. Lemberg. 2003. Controlling Storm-Water Runoff with Tradable Allowances for Impervious Surfaces. *Journal of Water Resources Planning and Management,* 129**:** 409-418. DOI: doi:10.1061/(ASCE)0733-9496(2003)129:5(409)

VA SYD. 2013. Dagvattenstrategi för Lunds Kommun (Stormwater strategy for Lund Municipality). Retrieved 2014-03-21, from. http://www.hojea.se/rapporter/Dagvattenstrategi_Lunds_kmn_130528.pdf

Vautard, R., and P. Yiou. 2009. Control of recent European surface climate change by atmospheric flow. *Geophysical Research Letters,* 36**:** L22702. DOI: 10.1029/2009GL040480

Veracka, M. 2013. Delivering better water quality: Rethinking storm water management. In *Energy and Sustainability Conference (IESC), 2013,* 1-6. Farmingdale, NY: IEEE.

Wilson, C. B., J. B. Valdes, and I. Rodriguez-Iturbe. 1979. On the influence of the spatial distribution of rainfall on storm runoff. *Water Resources Research,* 15**:** 321-328. DOI: 10.1029/WR015i002p00321

Zhou, Q., and X. Liu. 2004. Analysis of errors of derived slope and aspect related to DEM data properties. *Computers & Geosciences,* 30**:** 369-378. DOI: http://dx.doi.org/10.1016/j.cageo.2003.07.005

Zhou, Q., P. Pilesjö, and Y. Chen. 2011. Estimating surface flow paths on a digital elevation model using a triangular facet network. *Water Resources Research,* 47**:** W07522. DOI: 10.1029/2010WR009961

Institutionen för naturgeografi och ekosystemvetenskap, Lunds Universitet.

Student examensarbete (Seminarieuppsatser). Uppsatserna finns tillgängliga på institutionens geobibliotek, Sölvegatan 12, 223 62 LUND. Serien startade 1985. Hela listan och själva uppsatserna är även tillgängliga på LUP student papers (https://lup.lub.lu.se/student-papers/search/) och via Geobiblioteket (www.geobib.lu.se)
The student thesis reports are available at the Geo-Library, Department of Physical Geography and Ecosystem Science, University of Lund, Sölvegatan 12, S-223 62 Lund, Sweden. Report series started 1985. The complete list and electronic versions are also electronic available at the LUP student papers (https://lup.lub.lu.se/student-papers/search/) and through the Geo-library (www.geobib.lu.se)

335 Fei Lu (2015) Compute a Crowdedness Index on Historical GIS Data- A Case Study of Hög Parish, Sweden, 1812-1920
336 Lina Allesson (2015) Impact of photo-chemical processing of dissolved organic carbon on the bacterial respiratory quotient in aquatic ecosystems
337 Andreas Kiik (2015) Cartographic design of thematic polygons: a comparison using eye-movement metrics analysis
338 Iain Lednor (2015) Testing the robustness of the Plant Phenology Index to changes in temperature
339 Louise Bradshaw (2015) Submerged Landscapes - Locating Mesolithic settlements in Blekinge, Sweden
340 Elisabeth Maria Farrington (2015) The water crisis in Gaborone: Investigating the underlying factors resulting in the 'failure' of the Gaborone Dam, Botswana
341 Annie Forssblad (2015) Utvärdering av miljöersättning för odlingslandskapets värdefulla träd
342 Iris Behrens, Linn Gardell (2015) Water quality in Apac-, Mbale- & Lira district, Uganda - A field study evaluating problems and suitable solutions
343 Linnéa Larsson (2015) Analys av framtida översvämningsrisker i Malmö - En fallstudie av Castellums fastigheter
344 Ida Pettersson (2015) Comparing Ips Typographus and Dendroctonus ponderosas response to climate change with the use of phenology models
345 Frida Ulfves (2015) Classifying and Localizing Areas of Forest at Risk of Storm Damage in Kronoberg County
346 Alexander Nordström (2015) Förslag på dammar och skyddsområde med hjälp av GIS: En studie om löv- och klockgroda i Ystad kommun, Skåne
347 Samanah Seyedi-Shandiz (2015) Automatic Creation of Schematic Maps - A Case Study of the Railway Network at the Swedish Transport Administration
348 Johanna Andersson (2015) Heat Waves and their Impacts on Outdoor Workers – A Case Study in Northern and Eastern Uganda
349 Jimmie Carpman (2015) Spatially varying parameters in observed

new particle formation events

350 Mihaela – Mariana Tudoran (2015) Occurrences of insect outbreaks in Sweden in relation to climatic parameters since 1850

351 Maria Gatzouras (2015) Assessment of trampling impact in Icelandic natural areas in experimental plots with focus on image analysis of digital photographs

352 Gustav Wallner (2015) Estimating and evaluating GPP in the Sahel using MSG/SEVIRI and MODIS satellite data

353 Luisa Teixeira (2015) Exploring the relationships between biodiversity and benthic habitat in the Primeiras and Segundas Protected Area, Mozambique

354 Iris Behrens & Linn Gardell (2015) Water quality in Apac-, Mbale- & Lira district, Uganda - A field study evaluating problems and suitable solutions

355 Viktoria Björklund (2015) Water quality in rivers affected by urbanization: A Case Study in Minas Gerais, Brazil

356 Tara Mellquist (2015) Hållbar dagvattenhantering i Stockholms stad - En riskhanteringsanalys med avseende på långsiktig hållbarhet av Stockholms stads
dagvattenhantering i urban miljö

357 Jenny Hansson (2015) Trafikrelaterade luftföroreningar vid förskolor – En studie om kvävedioxidhalter vid förskolor i Malmö

358 Laura Reinelt (2015) Modelling vegetation dynamics and carbon fluxes in a high Arctic mire

359 Emelie Linnéa Graham (2015) Atmospheric reactivity of cyclic ethers of relevance to biofuel combustion

360 Filippo Gualla (2015) Sun position and PV panels: a model to determine the best orientation

361 Joakim Lindberg (2015) Locating potential flood areas in an urban environment using remote sensing and GIS, case study Lund, Sweden

362 Georgios-Konstantinos Lagkas (2015) Analysis of NDVI variation and snowmelt around Zackenberg station, Greenland with comparison of ground data and remote sensing.